universität wien

MASTERARBEIT / MASTER'S THESIS

Titel der Masterarbeit/ Title of the Master's thesis

Comprehensive evaluation of WRF-Chem simulations for a Saharan dust episode in spring 2018 with Earth observation data

verfasst von / submitted by
Katharina Perny, BSc

angestrebter akademischer Grad / in partial fulfillment of the requirements for the degree of
Master of Science (MSc)

Wien, September 2020 / Vienna, September 2020

Studienkennzahl lt. Studienblatt / degree programme code as it appears on the student record sheet:	UA 066 614
Studienrichtung lt. Studienblatt / degree programme as it appears on the student record sheet:	Masterstudium Metorologie
Betreut von / Supervisor:	Univ.-Prof. Mag. Dr. Leopold Haimberger

1 Abstract

The capability of the Weather Research and Forecasting model coupled with chemistry (WRF-Chem) to represent Saharan dust outbreaks has been investigated by applying two different settings to a case study of a dust episode in March/April 2018 in the Mediterranean Region. Two model configurations in WRF-Chem regarding their ability to simulate PM10 surface concentration and aerosol optical depth (AOD) were compared: The Goddard Chemistry Aerosol Radiation and Transport (GOCART) model with simple GOCART dust emission and the Modal Aerosol Dynamics Model for Europe (MADE) - Secondary Organic Aerosol Model (SORGAM) model with GOCART dust emission with Air Force Weather Agency (AFWA) modification.
The PM10 concentrations were validated against ground-based measurements of the European Environmental Agency (EEA) provided by the Zentralanstalt für Meteorologie und Geodynamik (ZAMG). Simulated AOD values were compared with Aerosol Robotic Network (AERONET) in Athens, Finokalia and Lampedusa, as well as European Aerosol Research Lidar Network (EARLINET) data from Athens. This data was collected from the respective online databases. Additionally the ZAMG provided Moderate Resolution Imaging Spectroradiometer (MODIS) data for the evaluation period, which was interpolated to allow a point evaluation.
Both model configurations tend to overestimate the observed PM10 concentrations with significantly larger errors shown by the GOCART configuration. The simulated PM10 pattern of the different models does not vary much. The major difference in magnitude between the models can be found over the desert area, hence, the emission source region.
The AOD observation datasets show many missing values due to the cloudy conditions over the Mediteranean Basin on this occasion and thereby complicate the evaluation. An overestimation of the models regarding their simulated AOD peaks and an underestimation of the background AOD when compared to AERONET was found. The background MODIS AOD values fit better to the model values while the peaks are also overestimated by both models. Due to the data availability issues the result should be interpreted with caution.

2 Zusammenfassung

Die Fähigkeit des Weather Research and Forecasting model coupled with chemistry (WRF-Chem) Saharastaubereignisse darzustellen wird anhand einer Fallstudie einer Saharastaubepisode im März/April 2018 über der Mittelmeerregion untersucht. Die Simulationen von PM10 Bodenkonzentrationen und Aerosol Optical Depth (AOD) von zwei WRF-Chem Modellkonfigurationen werden verglichen: Das Goddard Chemistry Aerosol Radiation and Transport (GOCART) Modell mit einfacher GOCART Staubemission und das Modal Aerosol Dynamics Model for Europe (MADE) - Secondary Organic Aerosol Model (SORGAM) Modell mit GOCART Staubemission mit Air Force Weather Agency (AFWA) Modifikationen.
Die PM10 Konzentrationen werden gegenüber bodengestützten Messungen der European Environmental Agency (EEA) validiert, welche von der Zentralanstalt für Meteorologie und Geodynamik (ZAMG) bereit gestellt werden. Die simulierten AOD Werte werden mit Messungen des Aerosol Robotic Network (AERONET) in Athen, Finokalia und Lampedusa, als auch mit European Aerosol Research Lidar Network (EARLINET) Daten von Athen verglichen. Diese Daten wurden von den jeweilgen Online-Datenbanken gesammelt. Weiters wurden Moderate Resolution Imaging Spectroradiometer (MODIS) Daten über die Evaluierungsperiode von der ZAMG zur Verfügung gestellt, welche zur Punktverifikation interpoliert werden.
Beide Modellkonfigurationen neigen dazu die beobachteten PM10 Konzentrationen zu überschätzen, wobei die GOCART Konfiguration deutlich höhere Fehler aufweist. Das zeitliche Muster der PM10 Konzentrationen unterscheidet sich nicht sehr unter den beiden Modellen. Der größte Unterschied zwischen den simulierten PM10 Konzentrationen kann über den Wüstenregionen gefunden werden, welche auch die primären Emissionsquellen für Staub darstellen.
The AOD Beobachtungsdaten weisen viele fehlende Werte wegen der bewölkten Bedingungen über der Mittelmeerregion zu dieser Zeit auf und machen die Evaluierung schwieriger. Eine Überschätzung der Modelle bezüglich der simulierten AOD Spitzen und eine Unterschätzung der Hintergrund AOD kann bei einem Vergleich mit AERONET Daten beobachtet werden. The Hintergrund AOD-Werte von MODIS passen besser zu den Modellsimulationen wobei ebenfalls die Spitzenwerte von beiden Modellen überschätzt werden. Wegen den Datenverfügbarkeitsproblemen sollten die Ergebnisse nur mit Vorsicht interpretiert werden.

Contents

List of Figures

List of Tables

Abbreviations

AERONET Aerosol Robotic Network.

AFWA Air ForceWeather Agency.

AOD Aerosol Optical Depth.

AVHRR Advanced Very High Resolution Radiometer.

CAPS Center for Analysis and Prediction of Storms.

EARLINET European Aerosol Research Lidar Network.

ECMWF European Center for Medium-Range Weather Forecast.

EEA European Environment Agency.

FAA Federal Aviation Administration.

GCM General Circulation Model.

GOCART Georgia Tech/ Goddart Global Ozone Chemistry Aerosol Radiation and Transport.

IFS Integrated Forecast System.

Lidar Light dedection and ranging.

MADE Modal Aerosol Dynamics Model for Europe.

MEGAN Model of Emissions of Gases and Aerosols from Nature.

MMM Mesoscale and Microscale Meteorology.

MODIS Moderate Resolution Imaging Spectroradiometer.

MOSAIC Model for Simulating Aerosol Interactions and Chemistry.

NAO North Atlantic Oscillation.

NASA National Aeronautics and Space Administration.

NCAR National Center for Atmospheric Research.

NCEP National Centers for Environmental Prediction.

NOAA National Oceanic and Atmospheric Administration.

NRL Naval Research Laboratory.

NWP Numerical Weather Prediction.

PBL Planetary Boundary Layer.

RPM Regional Particulate Model.

RRTMG Rapid Refresh Radiative Transfer Model for General circulation models.

SOA Secondary Organic Aerosol.

SORGAM Secondary Organic Aerosol Model.

WRF Weather Research and Forecasting Model.

ZAMG Zentralanstalt für Meteorologie und Geodynamik.

3 Introduction

Airborne dust is a key atmospheric constituent and its emissions in arid and semi-arid regions represent an important natural source of atmospheric particulate matter, which is a harmful air pollutant. Atmospheric dust can have severe effects on the human body with a direct relation to the the grain size. As particles decrease in size they increase their ability to penetrate into the lower airways, causing respiratory diseases and infections [Kim et al., 2015]. For preventing additional pollution through anthropogenic emissions of particulate matter the EU released restrictions of PM10 and PM2.5 emissions. For PM10 there are limit values for short-term (24 hour) and long-term (annual) exposure, while for PM2.5 there are only values for long-term (annual) exposure. A penalty fee must be paid if these limits are exceeded. Often natural phenomenons like Saharan dust outbreaks can lead to increased particulate matter values. In that case, model simulations are often used to prove the natural cause [Report, 2012].
In addition particulate matter forecasts are used to help authorities to warn the population and close public institutions in order to mitigate dust's impact on areas such as transportation, military operations, energy and health. Significant dust events can have a substantial economic impact as reduced visibility can affect air traffic and road transportation by closing roads and airports [Benedetti et al., 2013].
Furthermore dust has influence on different aspects of weather and climate dynamics, the Earth's radiative budget as well as cloud microphysics and atmospheric chemistry. These interactions are very important especially for climate modeling. Therefore, improvement of dust forecast in Numerical Weather Prediction (NWP) models is essentially for many purposes [Benedetti et al., 2013].

In this thesis the Weather Research and Forecasting model coupled with Chemistry (WRF-Chem) is used to simulate a Saharan dust outbreak in Spring 2018 which had severe effects on the island of Crete, where the local airport Iraklion had to be closed due to reduced visibility [Keep Talking Greece, 2020].
Two different settings regarding aerosol model and emission scheme were tested in order to evaluate the better representation of particulate matter on the surface and Aerosol optical depth at specific locations.
WRF-Chem has been used for simulating dust storms in previous studies for example over northern India ([Kumar et al., 2014]) and Egypt ([Eltahan et al., 2018]). The major findings are a overestimation of AOD in comparison with MODIS and AERONET data.
To evaluate the behavior of the different model settings PM10 is validated with an observation data set of the European Eviornmental Agency (EEA) of continuous PM10 measurements at the surface. AOD is compared to MODIS, AERONET und EARLINET measurements. First of all a brief description of the weather pattern over the Mediterenean Region in the time of the case study is given. The second chapter summarizes the theory of dust in the atmosphere and modelling of dust in NWP models. Afterwards follows a section about the WRF-Chem Model, the configuration and setup for the simulations and a description of the main differences between the two observed model configurations. The

next section includes a description of the different datasets and data preparation methods as well as statistical measurements used in this study. Afterwards, the results are given, followed by the discussion and a future scope.

3.1 Background

In the eastern Mediterranean, the dust events show a seasonality maximizing in spring due to the development of the Sahara depressions (also known as the Sharav Cyclone or Khasmin Depression). These depressions are formed especially in this time of the year because of the strengthening of the temperature gradient over northern Africa. They are generated south of the Atlas Mountains in Morocco and Algeria by the thermal contrast between cold Atlantic air and warm Saharan air and move eastwards along the north African coast affecting the central and eastern Mediterranean. With high frequency they can bring strong winds and sandstorms, transporting dust over long distances and affecting the Mediterranean Basin ([Kaskaoutis et al., 2019],[Bou Karam et al., 2010]). This type of dusty southerly wind is commonly known as "Khamsin".
The Sahara and its adjacent regions are the world's major source of aeolian mineral aerosol [Kaufman et al., 2005]. Dust gets predominately transported from North Africa to the eastern Mediterranean during spring and is often connected with the eastward movement of frontal low-pressure systems - Sharav cyclones. This spring cyclogenesis is explained by the lee effect as well as by the coastal thermal gradient which is due to the relatively colder oceanic waters to the north and warmer landmasses to the south. They move fast, more or less along the coastal line and are usually associated with an active cold front accompanied with rain. [Alpert and Ziv, 1989].
Long-range transport of the Saharan dust to the central Mediterranean is characterized by events lasting between 2 or 4 days, while an average duration of 1 day is usual for events reaching the eastern Mediterranean basin. In this area dry deposition seems to be dominant in comparison to wet deposition, especially in the summer months, when usually the dust concentrations are at a maximum and rainfall amounts are low [Goudie, 2006].

3.2 Description of the Sahara Dust Episode

As described in [Kaskaoutis et al., 2019], the negative North Atlantic Oscillation (NAO) phase (NAO index of -0.93) in March/April 2018 lead to increased cyclonic activity over nearly all of Europe, the western Mediterranean and northwest Africa. In the same areas the geopotential heights at several levels were much lower than the climatic values. In the contrary, a northward shift of the geopotential heights resulted in advection of warm air and higher geopotential height values in the eastern Mediterranean. Therefore, strong gradients in mean sea level pressure, geopotential heights and temperature were created between the western and eastern parts of the Mediterranean. This enabled the intensification of the westerly flow and favored the development and eastward movement of the Sharav cyclones along the north African coast and the Saharan dust intrusions towards the eastern Mediterranean. The intense dust storms on certain days (e.g., 17, 21-22, 25-26) in March

2018 were associated with strong surface, mid and upper-troposphere Khamsin winds in a cyclonic pathway, originated from Libya and transported northwards affecting Greece. The abnormally high Aerosol Optical Depth (AOD) values over the eastern Mediterranean were favoured by the deficit of precipitation, while increased rainfall occurred over the western parts of the Mediterranean [Kaskaoutis et al., 2019].
Crete, GR was severely affected by the Saharan dust outbreak on 3/22/2018, where PM10 concentrations exceeded 4 mm/m^3 (Iraklion - 4 mm/m^3, Finokalia - 5 mm/m^3), leading to the dusty conditions at the airport of Iraklion shown in Fig. 1.

Figure 1: Saharan dust outbreak in March 2018 in Crete. The photo was taken at Iraklio, 3/22/2018 14:50 local time. Copyright Mag.Mag. Renate Thumb

4 Dust in the atmosphere

Atmospheric aerosol is defined as the population of small, levitating liquid and solid particles dispersed in the air. Typically their size ranges from a few nanometers to about ten micrometers. The major aerosol constituents are mineral dust, sea salt, black and organic carbon, sulfate, nitrate, ammonium, and water. Atmospheric aerosol particles result from various sources, both, natural (i.e. sea spray, wind-driven release of desert dust, ...) and anthropogenic (such as the combustion of fuels or biomass burning) [Hendricks et al., 2012]. In principle, organic particulate matter can be divided into primary and secondary organic components. Primary organic aerosol is emitted directly into the atmosphere, whereas secondary organic aerosol (SOA) is formed in the atmosphere by gas-to-particle conversion. A schematic illustration of the life cycle of atmospheric aerosol is shown in Figure 2.
The distribution of trace compounds in the atmosphere depends on their sources (primary emission, chemical reactions as secondary sources), their sinks (chemical reactions, deposition) and the transport. Between the atmosphere and the contiguous reservoirs (i.e. biosphere, hydrosphere, kryosphere) exist various exchanges of material and energy. These complex feedbacks complicate the understanding of the ongoing processes on the one hand and the estimation of the anthropogenic effect on the atmosphere on the other hand [Möller, 2011].

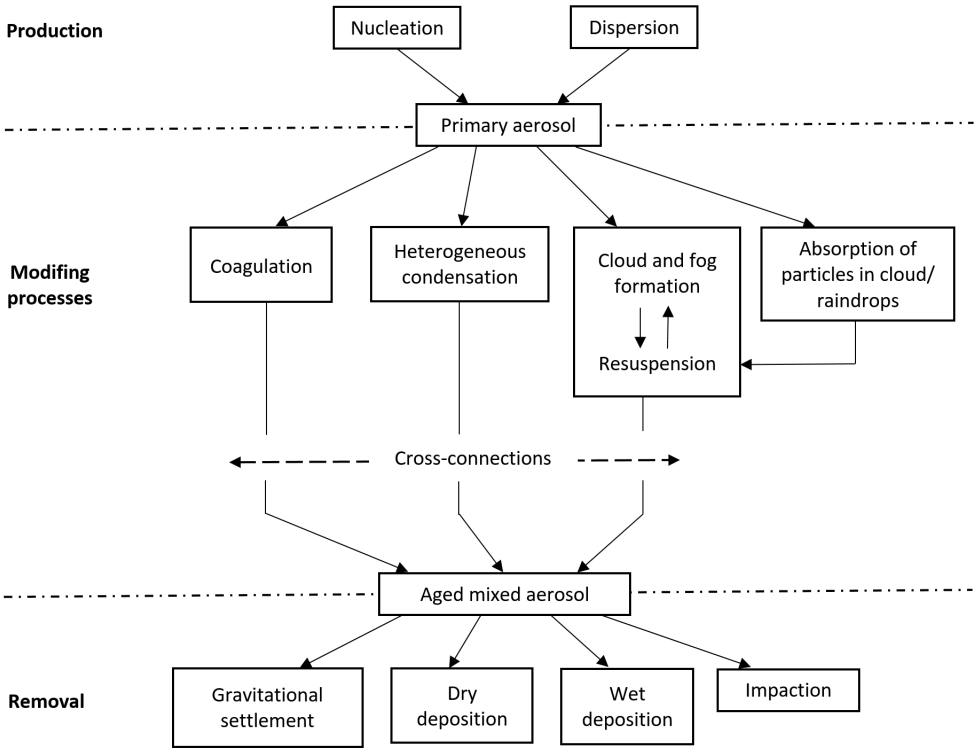

Figure 2: Schematic illustration of the life cycle of atmospheric aerosol.

4.1 Production of aerosol

In general, new particles can enter the atmosphere through two classes of mechanisms:

- by homogeneous condensation of supersaturated vapours from the gas phase (so-called homogeneous nucleation)
- by the dispersion and whirling up of material from the earth's surface, which is already there in condensed form, such as mineral dust or sea salt spray

Homogeneous condensation or nucleation describes the process in which a new droplet is formed by statistical collision of vapour molecules in a previously pure gaseous medium. This requires high supersaturations of up to several hundred percent which usually cannot be obtained in the troposphere. On the other hand, in a system with two or even more components involved, a so-called heteromolecular system, much higher supersaturations can occur for a given concentration of a species if the mixture of components is exothermic. In such a case, the saturation vapour pressure of a component above the mixture can be orders of magnitude lower than above the single component. Homogeneous nucleation in the atmosphere is important for the formation of aerosol droplets (e.g. from sulphuric acid). An alternative to homogeneous nucleation is heterogeneous nucleation, thus, condensation on already existing particles. If the diameters of the existing particles are sufficiently large (this is usually the case), only a small supersaturation is required for heterogeneous condensation [Roedel and Wagner, 2011].

A multitude of processes that are difficult to survey is involved in the production of aerosols due to dispersion. From the amount of particles produced, two mechanisms are of particular interest: the whirling up of mineral dust and the production of sea salt particles [Roedel and Wagner, 2011].

The production of sea salt aerosols is due to the blasting of bubbles on the sea surface which form due to strong wind in the crest of the breaking waves. This mechanism takes place around wind speeds $> 3\ ms^{-1}$. Two kinds of particles are formed. When the bubble bursts, on one hand, a large amount of small drops is created by the bursting of the bubble. On the other hand, due to the surface tension of the water a central jet rises which dissolves into about 3 to 8 droplets that can be thrown up several centimeters. The concentration rapidly increases with distance to the sea surface [Roedel and Wagner, 2011].

Regarding surface dust, it can be distinguished between erosion through wind and resuspension through anthropogenic activity, for instance traffic. Surface dust is created by chemical and mechanical weathering processes which form a huge amount of small grains out of the surface material. These are then further crushed into a spectrum of different grain sizes. Surface structure, surface moisture and wind speed are the key parameters for wind erosion. Emissions of dust in arid and semi-arid regions represent an important natural source of atmospheric particulate matter which is considered to be a harmful air pollutant. Locally surface dust can make a significant contribute to the atmospheric dust pollution. Dust storms/episodes occur episodically and last less than an hour and rarely

one to few days [Heintzenberg, 1994].
Soil particles mobilize when lift, drag and impact forces overcome gravitational and inter-particle cohesive forces. For the entrainment of atmospheric dust particles three processes are important: (1) aerodynamic lift, (2) saltation bombardment, and (3) particle disaggregation [LeGrand et al., 2019].
Aerodynamic lift (1), where wind shear forces directly act upon dust particles at the surface, is most efficient at lifting larger particles, e.g. fine sand grains. Due to the fact that cohesive forces on particles smaller than 60-70 μm are generally much larger than aerodynamic forces, dust-sized ($>$ 0.1-10 μm) particles are rarely lofted directly by the wind. Particles on the order of 60-70 μm are the first to be lifted as wind speeds increase [LeGrand et al., 2019].
Once detached from the ground, the larger particles undergo saltation, thus the process in which lifted particles fall back upon the surface because they are too heavy to remain in the air. Dust emission by saltation bombardment (2) takes place, when the impact energy from collision with the surface engages new particles in saltation and imports sufficient force to overcome the gravitational and cohesive forces binding particles to the ground. Saltation bombardment is the most common process for the emission of smaller dust-sized particles [LeGrand et al., 2019]. Particle disaggregation (3) is similar to the previous emission mechanism but instead of collisions mobilizing dust particles form the soil surface, the dust emitted is part of the saltating particle. It may for example originate from dust coatings on solid particles or clay aggregates disintegrating during collision. The disaggregation process can be a significant source under certain soil conditions. [LeGrand et al., 2019].

4.2 Aerosol modifying processes in the atmosphere

From Fig. 2 it can be seen that the primary aerosol is changed by different aerosol physical and meteorological processes. This includes the previous mentioned heterogeneous condensation as well as the process of coagulation mainly driven by the Brownian motion of the particles. Thereby, collision and sticking of aerosol particles leads to the formation of larger particles. Furthermore, the surface of liquid aerosols experiences an exchange of molecules with the gas phase. This can lead to condensation and subsequently to cloud and fog formation as well as resuspension and re-evaporation into the gas phase [Hendricks et al., 2012].

4.3 Deposition of trace compounds

The distance traveled by aerosols especially dust particles depends upon many factors, including grain characteristics, wind speed and turbulence and their settling velocity, the latter depending on the mass and shape of each particle [Goudie, 2006]. The discharge of substances from the atmosphere is called deposition and happens according to four different physical principles:

- **sedimentation** of substance due to gravity,
- **sorption** of substance on the earth's surface and a resulting transport process - vertically downwards - (dry deposition),
- by **sorption** and/or **impaction** of substance to falling hydrometeors and
- from a flowing mass of air by **impaction** of particles on surfaces.

Gravitation only has an effect on particles $> 5\mu$m and is also the physical processes responsible for the deposition of hydrometeors (precipitation). The discharge of substances by rain, snow and other solid hydrometeors is called wet deposition [Möller, 2011].

Wet deposition is an event-related process in contrast to all other continuous deposition processes. In the sense of a material flow it includes the sum of all wash-out mechanisms [Möller, 2011]. Wet deposition can occur in two ways: on one hand below the cloud, when raindrops, snowflakes or hailstones scavenge dust as they fall (sub-cloud scavenging), and on the other hand within a cloud, as water droplets capture dust particles and descended to earth when the precipitation falls (in-cloud scavenging). It can sometimes be manifested in the phenomenon of 'blood rains' and can be measured directly [Goudie, 2006]. The absorption of aerosol particles in the falling raindrop is always considered irreversible. The mechanisms (Brownian diffusion, interception, impaction) of particle transport in the drop environment are strongly dependent on the drop radius [Möller, 2011].

The process of dry deposition can be broken down into the following sub-steps:

a) aerodynamic (turbulent) transport through the atmospheric surface layer to a molecular boundary layer at the surface,

b) molecular transport (for molecules only) or Brownian transport (for particles only) through the interface to the surface,

c) absorption by the surface.

Each substep contributes to the value of the deposition rate. The absorption by the surface occurs for gases by sorption, for particles by adhesion, and for gases and particles actively by respiration and air exchange via stomata of plant leaves. In addition to chemical and physical processes on the surface, biological and biochemical conditions also determine the absorption of substances and thus the (negative) concentration gradient forming towards

the earth's surface. Only the concentration gradient is ultimately the driving force for the vertically downward transport. If the plant or the soil itself is the emittent of the regarded component, it is possible that an upward gradient of emission counteracts the downward gradient of dry deposition. If both material flows are of the same size, the compensation point is achieved. Experimentally, the two material flows cannot be separated, only the net flow can be measured. Therefore it is important to know the dependencies of the compensation point, including for example temperature and soilmoisture [Möller, 2011]. Dry deposition is normally estimated by measuring aerosol dust concentration and settling velocities [Goudie, 2006].

Within a flowing air mass, molecules and small particles move around obstacles according to the air flow. Larger particles, however, based on their inertia, will keep direction of their initial movement and therefore will not flow around obstacles but will collide with them. This process is called impaction. If particles and obstacle are of comparable size, a particle can also be captured from the particle-air trajectory if it passes close enough to the obstacle. This process is called interception. It has a very low effect compared to impaction [Möller, 2011].

Sedimentation and wet deposition depend only on atmospheric parameters and are completely independent of the earth's surface conditions. Dry deposition and impaction instead, depend on both, atmospheric variables and the characteristics of the surface. From previous knowledge of the close interconnection of wet deposition with the complex processes of precipitation formation, cloud chemical processes, it can be concluded that no linear relationship can exist between emission and wet deposition. The dry deposition is directly dependent on the gas phase concentration gaseous and particle-like substances. Therefore, dry deposition near the emission sources plays a much greater role in terms of quantity than wet deposition, which on the other hand becomes dominant at a greater distance from the sources. This is an expression of the fact that trace substances dissolved in clouds can be transported over long distances to remote areas that are less polluted by gaseous and particulate trace substances. In very arid areas, when the probability of precipitation is extremely low, dry deposition and sedimentation (mostly from ground dust) dominate [Möller, 2011].

4.4 Modelling of aerosols

Aerosol models are used to study the distribution and properties of atmospheric aerosol particles and their effects on clouds, atmospheric chemistry, radiation, and climate. They usually include a number of submodels to represent the different processes affecting atmospheric aerosols. Microphysical processes, particulary aerosol-aerosol and aerosol-gas phase interactions which affect the aerosol size distribution on the microscale are often subsumed within a specific submodel. Other processes like chemical transformations, atmospheric transport, wet and dry deposition of particles are mostly simulated by other submodules [Hendricks et al., 2012].

4.4.1 Aerosol type and size distribution

The model should provide information about the atmospheric mass concentration of different aerosol types, the aerosol particle number concentration as well as the particle size distribution. The first generation of aerosol models considered only the mass concentration of some aerosol constituents. With increasing computer power, more comprehensive models have been implemented, which also enable the simulation of particle number concentration and size distribution or even consider large numbers of individual size bin (bin schemes) or track the size and composition of individual particles (particle-resolved models). The latter would require very large computing resources, hence, large-scale aerosol models apply simplified size distribution [Hendricks et al., 2012].
As a common simplification, the aerosol size distribution is approximated by a superposition of several so-called size models. In many models, each mode is represented by a log-normal distribution, that is, a bell-shaped function in a coordinate system with a logarithmic abscissa:

$$n(\ln D) = \frac{N_t}{d \ln D} = \frac{N_t}{\sqrt{2\pi} \ln \sigma} \exp[-\frac{(\ln D - \ln D_{med})^2}{2 \ln^2 \sigma}] \tag{1}$$

where, N_t is the total particle number concentration of the mode, D is the particle diameter, σ is the geometric standard deviation describing the width of the mode, and D_{med} is the median diameter, where log-normal function in the form of Equation 1 shows its maximum value [Hendricks et al., 2012].
The size distribution of tropospheric aerosol can be approximated by a superposition of three log-normal modes covering the particle size ranges of a few nanometers (nm) to about 100 nm (Aitken mode), about 100 nm to 1 micrometer (μm) (accumulation mode), and about 1 μm to several 10 μm (coarse mode), demonstrated by [Whitby, 1978]. Current aerosol models that apply log-normal approach often consider more than three log-normal modes. On the basis of measured size distributions, some models include an additional mode, the nucleation mode, to separate very fine particles in the size range of a few nanometers from the Aitken mode [Hendricks et al., 2012].

4.4.2 Aerosol microphysical processes

The production of aerosols through nucleation results in an increase of particle number and mass concentration. These are assigned to the finest-sized mode in NWP-models. Parameterizations usually describe the nucleation of particles containing sulfuric acid (H_2SO_4) and water [Hendricks et al., 2012].
Regarding condensation/evaporation, in NWP-models a distinction between low- and high-volatile compounds is made. Usually it is assumed that evaporation of low-volatile compounds is negligible and for simulating condensation particle-size-dependent physical descriptions of the gasfluxes to the particle surfaces are applied. For constituents with higher volatility it is often considered that within the time step used in the model condensation and evaporation reach an equilibrium. This has the advantage that fluxes of con-

densed/evaporated particles do not have to be physically described but only the equilibrium partitioning between gas and particles has to be determined. In many cases, however, such fluxes are explicitly calculated [Hendricks et al., 2012].
Modal approaches of NWP-models consider coagulation of particles from the same mode (intramodal coagulation) as well as coagulation of particles from different modes (intermodal coagulation). Intramodal coagulation leads to a reduction of the particle number concentration in the respective mode, while intermodal coagulation results in a reduction in the smaller-sized mode and a corresponding transfer of mass from the smaller-sized to the larger-sized mode [Hendricks et al., 2012].

4.4.3 Emission and chemical transformation

The representation of emission of aerosol and its precursors in numerical models depends on the specific emission process [Hendricks et al., 2012].
A dust emission scheme must account in some way for (at least) the second and third emission mechanisms (saltation bombardment and disaggregation; see previous chapter 4.1) to represent dust production processes. This requires the representation of mobilization of saltating grains due to wind shear (aerodynamic lift), the transfer of energy from saltating grains to dust particle ejection and the resistance of the soil to sandblasting during collisions. Due to the requirement of correctly modeling (1) wind shear mobilization of larger particles and (2) bombardment interactions between particles of different sizes it can be difficult to create a model for saltation bombardment. For modeling the disaggregation process a priori knowledge of soil conditions is necessary [LeGrand et al., 2019].

Chemical transformation of aerosol precursors can be simulated with the aid of gas and liquid phase chemistry schemes. Due to the high computational costs of these schemes, many NWP- models consider only simplified aerosol precursor chemistry with a limited number of reactions and species [Hendricks et al., 2012].

4.4.4 Transport and deposition

NWP - models use transport schemes to simulate the transport of aerosol, its precursor gases, and other components relevant for the aerosol simulation. These schemes differ depending on the kind of transport they want to describe. The three main categories are large-scale wind systems (advection), small-scale vertical motions driven by local heating of air masses (convection), and small-scale turbulent motion (diffusion). Wind and other parameters relevant for these calculations are either prescribed or calculated. If these parameters are calculated by the model it is called online calculation and enables the quantification of effects of aerosols on weather, whereas prescribed meteorology simplifies the model system but enables only passive aerosol transport [Hendricks et al., 2012].

The process of wet deposition is simulated by NWP-models by coupling aerosol modules to cloud and precipitation schemes. By combining the information of aerosol modules about the relevant aerosol properties and of cloud and precipitation schemes about cloud

coverage and cloud microphysical properties as well as the precipitation formation rates and precipitation fluxes, the amount of aerosol removed from the atmosphere through wet deposition can be calculated. Dry deposition, however, is commonly expressed in terms of a deposition velocity which can be approximated by a function of particle size and composition as well as by local aerodynamic and surface properties [Hendricks et al., 2012].

4.4.5 Simulation of aerosol effects on atmosphere and climate

Aerosols have an effect on the Earth's radiation budget, influencing weather and climate, therefore, NWP- and especially GCM-models include submodels which consider absorption and scattering of radiation by atmospheric aerosols. Furthermore, they serve as condensation nuclei in the development of cloud drops and ice crystals and their interaction with radiation can effect cloud properties and lifetime. In addition, aerosols interactions can lead to the transformation of gases in the atmosphere which can be considered by using gas phase chemistry schemes [Hendricks et al., 2012].

4.5 Measurement

4.5.1 Particulate Matter (PM)

Aerosols consist of ordinary dust, smoke, soot and particles generated by condensation and re-sublimation of oversaturated gases and chemical processes. They are distinguished by particle size or composition [DWD, 2020].
The so called coarse particulate matter (PM10) particle fraction includes 50% of the particles with a diameter of 10 μm, a higher proportion of smaller particles and a lower proportion of larger particles. PM10 can penetrate the deepest part of the lungs. Similarly, so called fine particulate matter (PM2.5), can even reach the gas exchange regions of the lung, as well as very small particles (ultrafine particulate matter, PM0.1) may pass through the lungs to affect other organs [Umweltbundesamt, 2020].

4.5.2 Aerosol optical depth (AOD)

The aerosol optical depth (AOD) τ describes the exponential attenuation of incoming solar radiation through the atmosphere by particles according to Lambert-Beer law:

$$I(\lambda) = I_0(\lambda) \exp[-\tau(\lambda)], \tag{2}$$

where $I_0(\lambda)$ and $I(\lambda)$ are the intensities of incoming radiation on top of the atmosphere and on ground at wavelength λ. The AOD equals the vertical integration of extinction over the entire atmospheric column. Describing the impact of aerosols on weather and climate, the AOD is the main aerosol parameter used in radiative transfer simulations and is furthermore the only aerosol parameter that can be assimilated operationally with reasonable spatio-temporal resolution into global dynamic NWP models [DWD, 2020].

5 The Weather Research & Forecasting (WRF) Model

5.1 WRF-Chem

The WRF model is a numerical weather prediction (NWP) and atmospheric simulation system designed for both research and operational applications. The development of the WRF model has been a multi-agency effort, among them the National Center for Atmospheric Research's (NCAR) Mesoscale and Microscale Meteorology (MMM]) Division, the National Oceanic and Atmospheric Administration's (NOAA) National Centers for Environmental Prediction (NCEP) and Earth System Research Laboratory (ESRL), the Department of Defense's Air ForceWeather Agency (AFWA) and Naval Research Laboratory (NRL), the Center for Analysis and Prediction of Storms (CAPS) at the University of Oklahoma, and the Federal Aviation Administration (FAA), with the participation of university scientists. WRF contains a flexible, state-of-the-art, portable code that is efficient in computing environments and can be configured for both research and operational applications. Further multiple physical and dynamical options can be chosen [Skamarock et al., 2008].

The WRF-Chem model is an implementation of a fully coupled online chemistry in the WRF model. The air quality component of the model is fully consistent with the meteorological component. Both use the same transport, grid and physics schemes for subgrid-scale transport and they also use the same timestep, hence, no temporal interpolation is needed [Grell et al., 2005]. The dry deposition is coupled with the soil/vegetation scheme and the aqueous phase chemistry is coupled to some of the microphysics and aerosol schemes. There is a choice between three aerosol schemes: The Modal Aerosol Dynamics Model for Europe (MADE/SORGAM), Model for Simulating Aerosol Interactions and Chemistry (MOSAIC) and The Georgia Tech/ Goddart Global Ozone Chemistry Aerosol Radiation and Transport (GOCART) model [Skamarock et al., 2008]. The purpose of this thesis is a comparison between the MADE/SORGAM model and the GOCART model, which are going to be discussed in detail in the next sections.

Atmospheric process	Scheme
Cloud microphysics	Morrison double moment ([Morrison et al., 2005])
Cumulus parameterization	Grell ensemble cumulus scheme (G3; [Grell and Freitas, 2013])
Land surface physics	NOAH Land surface model ([Chen and Dudhia, 2011])
Surface layer	MYNN ([Morrison et al., 2009])
Planetary boundary layer	MYNN 2.5 ([Nakanishi and Niino, 2006])
Short - and longwave radiation	RRTMG scheme ([Iacono et al., 2008])

Table 1: Physics options used and common in all simulations

5.1.1 Model setup and configuration

This study uses the version version 3.4.1 of the WRF Model ([Skamarock et al., 2008]) coupled with chemistry ([Grell et al., 2005]) to simulate the meteorology and chemistry over the model domain shown in Fig. 3. The model domain is defined on a Mercator projection and extends from North-Africa over whole Europe to Greenland at a horizontal grid spacing of 12 x 12 km^2. Analysis and forecast data (resolutions- (1) horizontal: 0.25 °, (2) vertical: 91 model levels, and (3) temporal: 3 hourly) provided by the global Integrated Forecast System (IFS) model operated at the European Center for Medium-Range Weather Forecast (ECMWF) were used to initialize the model.
Table 1 provides a summary of the physics setting commonly used in the simulations. The resolved scale cloud physics is represented by the Morrison cloud microphysics scheme ([Morrison et al., 2005]) and sub-grid scale effects of convective and shallow clouds are parameterized according to the new Grell scheme ([Grell and Freitas, 2013]). The short- and long-wave radiative transfer in the atmosphere is represented by the Rapid Refresh Radiative Transfer Model for General Circulation Models (RRTMG) ([Iacono et al., 2008]), which allows online interaction between aerosols and meteorology in the model. For surface processes, the model setup uses the NOAH Land surface model ([Chen and Dudhia, 2011]) and MYNN surface layer scheme ([Morrison et al., 2009]). The vertical sub-grid scale fluxes due to the eddy transport in the planetary boundary layer (PBL) and the free troposphere are parameterized according to the MYNN 2.5 TKE boundary layer scheme ([Nakanishi and Niino, 2006]).

Biogenetic emissions of trace species from terrestrial ecosystems are calculated online using the Model of Emissions of Gases and Aerosols from Nature (MEGAN) version 2.04 ([Guenther et al., 2006]). The study focuses on a comparison of two different aerosol models and different dust emission schemes. An overview of the different settings is given in Table 2. One configuration, here referred to as GOCART configuration, uses the (GO-

Atmospheric process	GOCART setting	MADE setting
Chemistry	GOCART simple/ no ozone chemistry chem_opt = 300	RADM2 - MADE/SORGAM chem_opt = 11
Background emissions	GOCART simple emiss_opt = 6	GOCART RACM_KPP emiss_opt = 5
Dust emission	GOCART dust emission dust_opt = 1	GOCART with AWFA modification dust_opt = 3
Photolysis	no photolysis phot_opt = 0	Fast-J photolysis phot_opt = 2

Table 2: Differences in the chemistry settings of the simultations

CART) Model([Chin et al., 2000]) as aerosol model and the GOCART dust emissions, with this configuration no photolysis is possible. For the second configuration, as of here, MADE configuration, the MADE/SORGAM ([Ackermann et al., 1998],[Schell et al., 2001]) model is applied for aerosol simulation and GOCART Air Force Weather Agency (AFWA) dust emissions are used. Photolysis was included according to the Fast-J photolysis scheme [Wild et al., 2000].
A 32-day period from March 17 until April 18, 2018, was simulated with WRF-Chem as a sequence of daily time slices with a previous spin-up of 5 days. The initial chemical state at the beginning of each time slice was adopted from the final state of the previous time slice, while meteorology was re-initialized with ECMWF analysis every day.

Figure 3: The WRF-Chem model domain.

5.1.2 Aerosol model

This chapter provides a brief overview of the aerosol models used in this study. A focus was put on the most important features and they will not be discussed in detail.

5.1.2.1 Georgia Tech/ Goddart Global Ozone Chemistry Aerosol Radiation and Transport (GOCART) Model

The Georgia Tech/Goddard Global Ozone Chemistry Aerosol Radiation and Transport (GOCART) model uses a bulk scheme, which calculates only with the total mass of the aerosol components and therefore provides no information on particle size and concentration. The GOCART model simulates the mass of the major tropospheric aerosol components, including sulfate, dust, black carbon (BC), organic carbon (OC), and sea-salt aerosols. It is numerically very efficient but has no interaction with radiation, is not coupled with cloud processes and does not include secondary organic aerosols SOA [Kazil, 2009].

5.1.2.2 Modal Aerosol Dynamics Model for Europe (MADE) - Secondary Organic Aerosol Model (SORGAM)

The aerosol module is based on the Modal Aerosol Dynamics Model for Europe (MADE) [Ackermann et al., 1998] which itself is a modification of the Regional Particulate Model (RPM)
[Binkowski and Shankar, 1995]. SOA have been incorporated into MADE by means of the Secondary Organic Aerosol Model (SORGAM) [Schell et al., 2001].
The Modal Aerosol Dynamics model for Europe (MADE) has been developed as an extension to mesoscale chemistry transport models by modeling particle formation, transport and deposition with respect to aerosol chemistry as well as aerosol dynamics. The particle size distribution of the submicrometer aerosol is represented by two overlapping log-normal modes. The assumed distribution is given in Equation 3.

$$n(\ln d_p) = \frac{N}{\sqrt{2\pi}\ln\sigma_g}\exp[-\frac{1}{2}\frac{(\ln d_p - \ln d_{p_g})^2}{\ln^2\sigma_g}], \tag{3}$$

where N is the number concentration [m^{-3}], d_p the particle diameter, d_{p_g} the median diameter, and σ_g the standard deviation of the distribution. This technique takes advantage of the modal structure of aerosol populations observed in the atmosphere (see Chapter 4.4.1).
Aerosol particle sources are modeled through nucleation and emission. As processes modifying the aerosol population, coagulation, condensation, transport and deposition are considered in this model. Aerosol dynamics calculations are performed on-line within the chemistry-transport model, in this case WRF-Chem. [Ackermann et al., 1998]
The prognostic variables (related to aerosols) which are transported in WRF-Chem are the total number of aerosol particles within each mode as well as all primary and secondary

species (organic and inorganic) for both Aitken and Accumulation mode and three species for the coarse mode (anthropogenic, marine, and soil-derived aerosols). Except for nucleation, where only inorganic compounds are considered, all aerosol dynamics processes include both inorganic and SOA compounds [RUC - NOAA, 2020].
The SORGAM was developed by [Schell, 2000]. When coupled to a comprehensive chemistry-transport model, the model is capable of simulating the formation of low-volatility products and their gas/particle partitioning [Schell et al., 2001].

5.1.3 Dust emission schemes

Two different dust emission schemes are used for the simulations, which are going to be discussed regarding their main differences in the following section. The here referred to as GOCART-WRF dust emission scheme (dust_opt =1) is applied in the GOCART setting, while GOCART emissions with AFWA modification (dust_opt = 3) are used in the MADE configuration. For a very detailed description see [LeGrand et al., 2019].

5.1.3.1 Simple GOCART dust emission

The Simple GOCART dust emission scheme was first incorporated into WRF-Chem version 3.2. and is based on the original GOCART scheme described in [Ginoux et al., 2001]. The original GOCART dust emission does not require soil or surface characteristics which would be difficult to obtain to run and is therefore popular with the modeling community. Wind speed, soil moisture, air density, and generalized soil traits are the only necessary inputs for its dust emission flux calculation.
The scheme is relatively simple and highly empirical as compared to other dust emission schemes due to a direct conversion from wind speed to dust emission. The physics of dust emission by saltation bombardment discussed in Section 4.1 would rather motivate using wind speed to calculate a saltating particle flux and then using this flux to determine dust emissions [LeGrand et al., 2019].
Emission flux values for each size bin (F_p; kg m^{-2}s^{-1}) are obtained using Equation 4.

$$F_p = \begin{cases} CSs_pU^2(U - u_t^*(D_p, \theta_s)), & U > u_t^*(D_p, \theta_s) \\ 0, & U \leq u_t^*(D_p, \theta_s) \end{cases}, \tag{4}$$

where C is a dimensional proportionality constant (default set to 0.8×10^{-9} kgs^{-1}m^{-5}), S is a unitless dust source strength function indicating availability of entrainable particles, s_p is the mass fraction of emittable dust from the soil separate class (i.e., sand, silt, or clay) of size group p at the soil surface, U is the horizontal wind speed at 10 m, and $u_t^*(D_p, \theta_s)$ is the friction velocity used as a threshold wind speed required for initiating erosion. In the original GOCART scheme ([Chin et al., 2000]) the threshold wind speed gets derived in terms of 10m wind speed, instead of friction velocity. Values of U are typically an order of magnitude, or more, greater than their equivalent u^*, which was not considered in the implementation in WRF-Chem. Until wind speeds are below a very low threshold emissions are not set to zero, which could lead to a false treatment of dust lifting at low

wind speeds [LeGrand et al., 2019].
The friction velocity is first derived for dry soil conditions based with an equation from [Marticorena and Bergametti, 1995], see Equation 5.

$$u_t^*(D_p) = 0.0013 \frac{(\frac{\rho_p g D_p}{\rho_a})^{0.5}(1 + \frac{0.006}{\rho_p g D^{2.5}})^{0.5}}{[1.928(a(D_p)^x + b)^{0.092} - 1]^{0.5}}, \tag{5}$$

where D_p is the particle diameter in bin p, g is acceleration due to gravity, ρ_p is the particle density in bin p, ρ_a is air density, $x = 1.56$, $a = 1331$ cm^{-x} , and $b = 0.38$.
A conditional statement is used to correct the threshold wind speed for soil surface wetness in terms of saturation, θ_s, see Equation 6. Soil moisture values passed in by the WRF-Chem framework are converted from volumetric water content (θ_v) to degree of saturation (θ_s) via $\theta_s = \theta_v/\phi$, where ϕ is the porosity of the soil medium.

$$u_t^*(D_p, \theta_s) = \begin{cases} u_t^*(D_p) \times (1.2 + 0.2 \log_{10} \theta_s), & \theta_s < 0.2 \\ \infty, & \theta_s \geq 0.2 \end{cases}. \tag{6}$$

S, the unitless dust source strength function used in the calculation of F_p in Equation 4, is added as a stand-in for soil surface characteristics necessary for describing availability of loose erodible soil material. A distinction is made between size bins that fall into the sand-sized category and those for the clay and silt category. The former are parameterized with $0.5S'$, the latter with $0.25S'$, where S' is given by Equation 7.

$$S = (\frac{z_{max} - z_i}{z_{max} - z_{min}})^5, \tag{7}$$

z_i is the elevation of the cell, and z_{max} and z_{min} are the maximum and minimum elevation in the surrounding $10° \times 10°$ area. For the calculation a $0.25°$ resolution elevation dataset, and the Advanced Very High Resolution Radiometer (AVHRR)-based vegetation mask were used [LeGrand et al., 2019].

5.1.3.2 GOCART AFWA dust emission

Equation 5 was originally not designed to represent the threshold for wind-shear-based emission of finer-grained dust particles from the surface but to determine the threshold for initiating wind-shear-based saltation. The AFWA scheme dust emission is handled as a two-part process wherein wind sheer triggers saltation of large particles which leads to fine-particle emission due to saltation bombardment. Similar to the Simple GOCART scheme particles are divided based on their effective size into nine saltations size bins and five dust size bins. Dust particle densities and effective diameters are consistent with those used in the Simple GOCART configuration. The diameters used in the following equations are denoted as $D_{s,p}$ and $D_{d,p}$ for the saltation and dust size bins [LeGrand et al., 2019].
Equation 5 from the Simple GOCART dust emission scheme is equally used in the AFWA schmeme to calculate the threshold friction velocity $u_t^*(D_{s,p})$ for the saltation process.

Similar to the Simple GOCART scheme, a correction function, $f(\theta)$ is applied to the threshold friction velocity to account for the effects of soil moisture on particle cohesion:

$$u^*_{t,s,p} = u^*_t(D_{s,p})f(\theta), \tag{8}$$

where

$$f(\theta) = \begin{cases} \sqrt{1 + 1.21(\theta_g - \theta'_g)^{0.68}}, & \theta_g > \theta'_g \\ 1, & \theta_g \leq \theta'_g \end{cases}. \tag{9}$$

θ_g is the gravimetric soil moisture fraction, and θ'_g is the fraction of soil moisture able to be absorbed before capillary forces begin to influence particle lifting. $theta_g$ gets derived by converting the volumetric water content (θ_v) soil moisture values provided by WRF-Chem [LeGrand et al., 2019].
Once time-varying $u^*_{t,s,p}$ values are known, the horizontal saltation flux equation (see Equation 10) is used to calculate the momentum transfer effects of wind shear and saltating grain impact shear.

$$H(D_{s,p}) = \begin{cases} \frac{\rho_a}{g} u_*^3 (1 + \frac{u^*_{t,s,p}}{u_*^2})(1 - \frac{{u^*_{t,s,p}}^2}{u_*^2}), & u_* > u^*_{t,s,p} \\ 0, & u_* \leq u^*_{t,s,p} \end{cases}, \tag{10}$$

The $H(D_{s,p})$ values are then integrated over particle sizes to obtain the total streamwise horizontal saltation flux (G) (see Equation 11).

$$G = \sum_{s,p} [H(D_{s,p}) dS_{rel}(D_{s,p})] \tag{11}$$

where $dS_{rel}(D_{s,p})$ are the saltation bin-specific weighting factors. To estimate the bulk emission flux of dust (F_B; g cm^{2}s^{-1}) triggered by saltation, the AWFA scheme utilizes the dust source strength parameterization and sandblasting efficiency approach (see Equation 12). A aerodynamic roughness length (z_0) conditional is also applied to limit dust emission to regions like grassland, sparsley vegetated or barren areas.

$$F_B = \begin{cases} GS\beta, & z_0 \leq 20\text{cm} \\ 0, & z_0 < 20\text{cm} \end{cases}, \tag{12}$$

where β is the sandblasting efficiency, which varies from 1.00×10^{-6} to 1.36×10^{-6}cm^{-3}, implying that the impact of the soil in the scheme is small.
The final size-resolved dust emission fluxes ($F_{d,p}$;g cm^{-2}s^{-1}) are obtained according to:

$$F_{d,p} = F_B \kappa_{d,p} \tag{13}$$

where $\kappa_{d,p}$ are the dust distribution weighting factors of each dust size bin.
As with the Simple GOCART scheme, the emitted dust particles are released into the lowest atmospheric model level for dispersion according to their respective size bins [LeGrand et al., 2019].

6 Methodology and Data

6.1 Observation datasets

6.1.1 European Environment Agency (EEA)

European-wide ground measurements from the European Environmental Agency (EEA) were used to evaluate the simulated PM10. The EEA's public air quality database system contains air quality monitoring data and information submitted by participating countries throughout Europe. The air quality database consists of a multi-annual time series of air quality measurement data and statistics for a number of pollutants. It also contains meta-information on those monitoring networks involved, their stations and their measurements. The database covers geographically all EU Member States, the EEA member countries and some EEA candidate countries [European Environment Agency, 2019].
The data and information regarding the observation stations were provided by the ZAMG, as well as the measurements from Crete (Finokalia and Iraklio), which were collected and received separately. PM10 measurements are available from 3/28/2018 0000 UTC to 4/14/2018 2300 UTC. For the evaluation a selection of sites in the eastern Mediterranean Region which recorded increased values of PM10 (more than 100 μg/m^3)was made. In Figure 4 the stations choose for the evaluation are shown in blue dots.
Depending on the predominant emission sources, stations are classified as follows:

- traffic stations - located in close proximity to a single major road;
- industrial stations - located in close proximity to an industrial area or an industrial source;
- background stations - pollution levels are representative of the average exposure of the general population or vegetation.

Further, the station can be classified depending on the distribution and density of buildings, as well as the area surrounding:

- urban - continuously built-up urban area;
- suburban - largely built-up urban area;
- rural - all other areas [European Environment Agency, 2019].

All used observation sites with information about their predominant location source, location class and their coordinates are given in Tbl. 3.

Station ID / Name	Latitude	Longitude	Location	Predominant emission
BG0018A	41.636080	25.37968	urban	background
BG0019A	43.411800	24.61501	urban	traffic
BG0038A	43.268210	26.93844	urban	background
BG0040A	42.732290	23.31097	urban	background
BG0044A	42.518890	27.37514	suburban	industrial
BG0050A	42.680560	23.29679	urban	background
BG0057A	43.126470	25.69121	urban	background
BG0058A	42.001930	23.09782	suburban	background
BG0066A	43.136920	24.71574	urban	background
BG0071A	42.659760	27.72096	urban	background
BG0073A	42.669800	23.26840	urban	traffic
IT0898A	40.854190	14.25133	urban	traffic
IT0934A	41.131460	14.78938	urban	traffic
IT1491A	40.853610	14.27167	urban	traffic
MK0030A	42.003610	21.46362	suburban	background
MK0031A	41.978330	21.47000	urban	industrial
MK0034A	41.913890	22.41585	urban	traffic
MK0035A	41.514450	20.95862	urban	industrial
MK0036A	42.135560	21.71474	urban	industrial
MK0037A	41.040000	21.35640	urban	industrial
MK0038A	41.030280	21.33667	urban	traffic
MK0040A	41.705830	21.76529	urban	traffic
MK0041A	42.004440	20.96807	urban	traffic
MK0043A	41.999170	21.44084	urban	traffic
MK0044A	41.440560	22.00723	urban	industrial
MK0045A	41.987440	21.65250	suburban	industrial
MK0048A	42.006000	21.38700	urban	background
MT00004	35.852290	14.53899	urban	background
MT00005	35.895840	14.48999	urban	traffic
MT00007	36.067070	14.19715	rural-regional	background
RS0032A	44.821120	20.45911	urban	background
Finokalia	35.337718	25.66975	unknown	unknown
Iraklio	35.330000	25.18000	unknown	unknown

Table 3: Classification of all stations used to evaluate PM10 concentrations

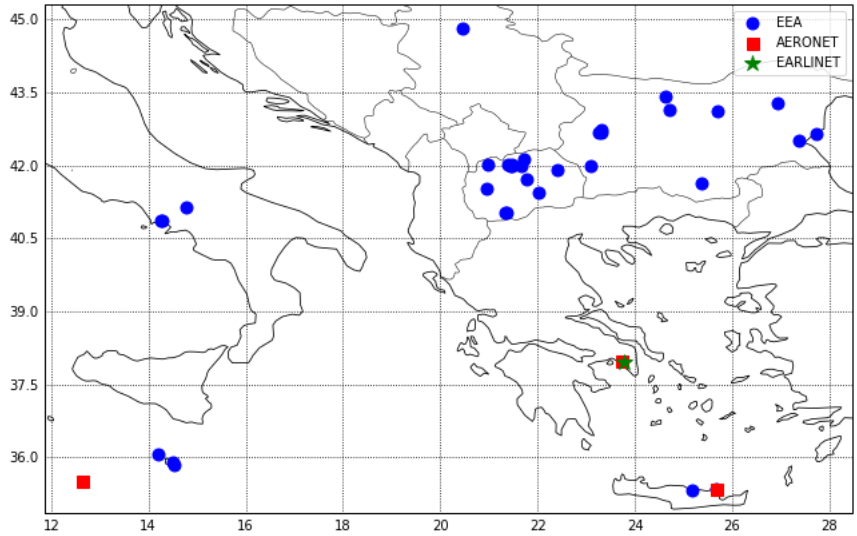

Figure 4: Location of observation stations: blue - EEA PM10 , red - AERONET AOD, green - EARLINET AOD

6.1.2 Aerosol Robotic Network (AERONET)

The Aerosol Robotic Network (AERONET) ([Holben et al., 1998]) is a ground-based remote sensing aerosol network of more than 100 sites established by the National Aeronautics and Space Administration (NASA), which uses Cimel Electronique Sun-sky radiometers to measure aerosol optical properties [Giles et al., 2018].
The data can be downloaded via a download tool at their homepage (`https://aeronet.gsfc.nasa.gov/cgi-bin/webtool_aod_v3`). There are three quality levels for AOD data retrieved and provieded by AERONET. Level 1.0 data, which is unscreend and may not have final calibration applied, level 1.5 which is automatically cloud cleared but may also not be calibrated and level 2.0 data which is additionally to the automatic cloud clearance manually inspected and where pre- and post calibration is applied [Giles et al., 2018].
For the evaluation period three measurement stations in the Mediterranean Region were active: Athens, GR (37.972N, 23.718E), Finokalia, GR (35.338N, 25.670E) and Lampedusa, IT (35.517N, 12.632E), the locations are shown as red squares in Fig. 4. For both, Athens and Finokalia Level 2.0 AOD measurements were available, whereas for Lampedusa only Level 1.5 data could be found.
Sun photometry is a passive remote-sensing measurement technique in which light, generally not scattered or absorbed by the atmosphere gets detected by a photodiode and converted to a digital signal. By using the Beer-Lambert-Bouguer law converted to instrument digital counts, seen in Equ. 14, the total optical depth can be determined .

$$V(\lambda) = V_0(\lambda) \cdot d^2 \cdot \exp[-\tau(\lambda)_{\text{Total}} \cdot m], \tag{14}$$

where $V(\lambda)$ is the measured spectral voltage dependent on the wavelength (λ), $V_0(\lambda)$ is the relative extraterrestrial spectral calibration coefficient dependent on λ, d is the ratio

of the average to the actual Earth-Sun distance, $\tau(\lambda)_{\text{Total}}$ is the cloud-free spectral total optical depth, and m is the optical air mass.
The spectral AOD ($\tau(\lambda)_{\text{Aerosol}}$) is computed from $\tau(\lambda)_{\text{Total}}$ and the subtraction of the contributions of Rayleigh scattering optical depth and spectrally dependent atmospheric trace gases as shown in Equ. 15 [Giles et al., 2018].

$$\tau(\lambda)_{\text{Aerosol}} = \tau(\lambda)_{\text{Reyleigh}} - \tau(\lambda)_{\text{H}_2\text{O}} - \tau(\lambda)_{\text{O}_3} - \tau(\lambda)_{\text{NO}_2} - \tau(\lambda)_{\text{CO}_2} - \tau(\lambda)_{\text{CH}_4} \tag{15}$$

6.1.3 European Aerosol Research Lidar Network (EARLINET)

Light detection and ranging (Lidar) remote sensing is the most appropriate tool to observe vertical concentrations of aerosols. Established in 2000, the European Aerosol Research Lidar Network (EARLINET) currently comprises 31 active stations distributed over Europe [EARLINET homepage, 2019]. A station is considered active when submitting aerosol extinction and/or backscatter coefficient profiles to the EARLINET database. The main objective of EARLINET is the development of a database to monitor the horizontal, vertical, and temporal distribution of atmospheric aerosol over the entire continent. The stations can be classified according to their capabilities into (1) Multiwavelength Raman-, (2) Raman- and (3) Backscatter- lidar stations [Pappalardo et al., 2014].
During the simulated period three multiwavelength Raman lidar stations located in the region of interest submitted measurements to the EARLINET database (`https://data.earlinet.org/`). In total there are three measurements available for Athens, GR (37.96N, 23.78E, 212 m) (3/29/2018 1725 and 1825 UTC and 4/16/2018 1824 UTC), one for Lecce, IT (40.33N, 18.10E, 30 m) (4/16/2018 1731 UTC) and one for Thessaloniki, GR (40.63N, 22.95E, 50 m) (4/09/2018 1005 UTC) [EARLINET homepage, 2019]. All three EARLINET stations suited for validation are collocated with AERONET sun photometers but only for Athens measurements are available, see section 6.1.2 above.
Due to the these availability issues and few measurements only the data for Athens were used for the evaluation.

6.1.4 Moderate Resolution Imaging Spectroradiometer (MODIS)

The goal of the Moderate Resolution Imaging Spectroradiometer (MODIS) instruments on board of the NASA Terra and Aqua satellites is to observe and monitor the Earth including tropospheric aerosols with high resolution and nearly daily global coverage. To characterize the global aerosol spectral radiances from 0.47 mm to 2.1 mm and independent algorithms over ocean and land are used [Kaufman et al., 2005].
The retrieval of aerosol properties over bright surfaces (e.g., Sahara desert) is challenging. The upward radiance recieved by the satellite is a composition of light from the solar beam scattered by the atmosphere and not reflected on the surface and the reflected parts of the direct and diffuse components. To overcome this problem, the so called "Deep Blue algorithm" has been integrated into the existing MODIS algorithm [Hsu et al., 2004].

The MODIS data for this study was provided by the ZAMG and is available over the whole simulation period.

6.2 Data preparation

6.2.1 WRF Simulations

To evaluate the simulations of WRF-Chem with observation data of ground stations the model data has to be interpolated to the coordinates of these sites.
To different methods have been tested to evaluate the difference between a computational expensive and a simpler approach. The computational expensive but more accurate implementation was an interpolation by using the python function **griddata** from the package **scipy.interpolate**.
The second option, simplifing the process, was to use the nearest gridpoint of the model grid to the coordinates to represent the simulation at that observation site. The Haversine formular (see Equation 16) was used to determine the distance between the wanted coordinates of the observation station and the gridpoint coordinates. The gridpoint with the smallest distance was taken as reference.

$$d = 2r \arcsin\left(\sqrt{\sin^2\left(\frac{\varphi_2 - \varphi_1}{2}\right) + \cos(\varphi_1)\cos(\varphi_2)\sin^2\left(\frac{\lambda_2 - \lambda_1}{2}\right)}\right) \tag{16}$$

where φ_1, φ_2 are the latitude of point 1 and latitude of point 2 (in radians), λ_1, λ_2 are the longitude of point 1 and longitude of point 2 (in radians).
To minimize computational costs the WRF domain was cut to a smaller one (see Fig. 5).

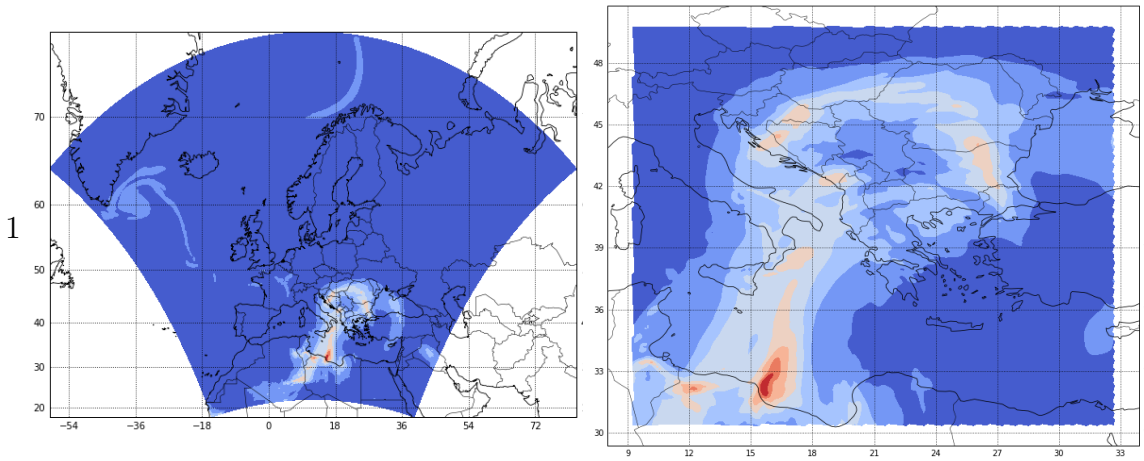

Figure 5: WRF-Chem simulation domain. Left: whole domain. Right: cut domain for interpolation

6.2.2 AERONET

The AERONET sunphotometers take measurements at specific wavelengths. The available stations Athens, Finokalia and Lampedusa measure at 340nm , 380nm, 440nm, 500nm, 675nm, 870nm and 1020nm, in Athens additionally at 1640nm. The measurement values increase monotonously from the lowest wavelengths at 1640/1020 nm to the highest at 340nm, as can be seen in Figure 6. Therefore, an interpolation to a wavelength of 550nm to compare it with WRF-Chem AOD at 550nm is possible.
The measurements of AERONET sites are not taken at fixed times, therefore a resampling had to be done. All values from the previous hour are averaged, e.g. all values measured between 13 and 14UTC are averaged and stored at 14UTC. Many missing values .

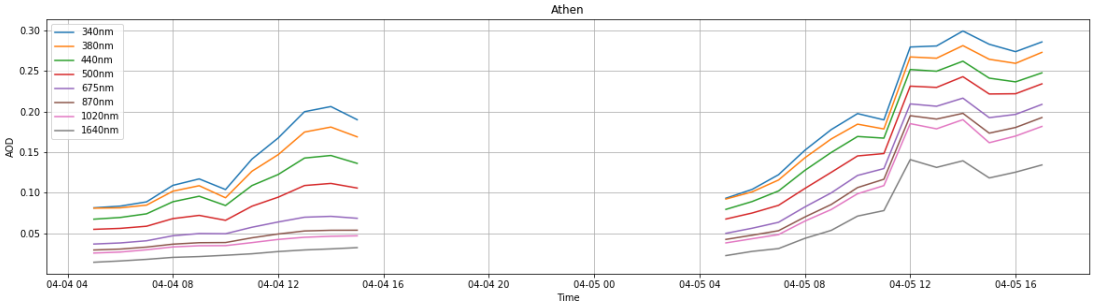

Figure 6: AOD measurements for different wavelengths from the AERONET station Athens from 4/4/2018 - 4/6/2018 00UTC

6.2.3 EARLINET

EARLINET observation stations measure the vertical profile of extinction. To retrieve AOD values an integration over the altitude of the aerosol extinction must be done.

$$AOD = \int_{h_0}^{h_1} \alpha(p)dp \tag{17}$$

Integrations are calculated with trapezoidal rule, where α_1,...,α_n are extinction values, and p_1,...,p_n are the corresponding altitudes at which extinction values are retrieved.

$$\int_{h_0}^{h_1} \alpha(p)dp \approx \sum_{j=1}^{n} \frac{\alpha_{j-1} + \alpha_j}{2} \cdot \frac{p_j - p_{j-1}}{2} \tag{18}$$

where $\alpha_0 = \alpha_1$ and $p_0 = l$, with l the station altitude [Ciamprone et al., 2019].

6.2.4 MODIS

The Aqua and Terra satellites each overpass the same area once a day taking measurements. The data shows many missing values due to post-processing steps like cloud-clearing, the coverage of the domain varies and due to the relatively short observation period a re-gridding onto the WRF simulation grid was not made. Instead, the MODIS data was interpolated with the nearest grid point method identically as with the WRF data to the observation site, where other AOD measurements were available, that are, Athens, Finokalia and Lampedusa. Additionally, because the MODIS data was the only data source where potentially more measurements were available, the data was interpolated to the coordinates of the PM10 observation sites as the WRF simulations were already interpolated there and, hence, the computational cost were not high.

6.3 Statistical values

6.3.1 Mean absolute error

The mean absolute error (MAE) is the arithmetic average of the absolute values of differences between forecast (y_k) and observation o_k.

$$\mathrm{MAE} = \frac{1}{n}\sum_{k=1}^{n}|y_k - o_k| \tag{19}$$

The MAE is zero if the forecasts are perfect (each $y_k = o_k$) and it increases as discrepancies between observation and forecast become larger. It can be interpreted as a typical magnitude of the forecast error.

6.3.2 Root mean square error

The mean squared error (MSE) is the averaged squared difference between the forecast and observation pairs. The square root of the MSE is called root mean square error (RMSE) and has the same physical dimension as the forecasts and observations, and can also be seen as typical magnitude of the forecast error. Due to the squaring of the forecast errors it is more sensitive to large errors than the MAE and ,therefore, is also more sensitive to outliers.

$$\mathrm{RMSE} = \sqrt{\frac{1}{n}\sum_{k=1}^{n}(y_k - o_k)^2} \tag{20}$$

6.3.3 Correlation

To measure the association between the forecast and the observation a correlation coefficient can be calculated. Usually, the "Pearson product-moment coefficient of linear correlation" between two variables x and y is meant when using the term *correlation coefficient*.

The Pearson correlation is defined as the ratio of the ample covariance of the variables to the product of their standard deviations.

$$r_{xy} = \frac{\mathrm{COV}(x,y)}{s_x s_y} = \frac{\frac{1}{n-1}\sum_{i=1}^{n}[(x_i - \overline{x})(y_i - \overline{y})]}{\left[\frac{1}{n-1}\sum_{i=1}^{n}(x_i - \overline{x})^2\right]^{1/2}\left[\frac{1}{n-1}\sum_{i=1}^{n}(y_i - \overline{y})^2\right]^{1/2}}, \tag{21}$$

where $\overline{x}$ denotes the mean of x.
The Pearson product-moment correlation coefficient is not robust because strong but non-linear relationships between variables may not be recognized. It is further not resistant due to its potentially extreme sensitivity to outliers.
The form of Eq. 21 requires two passes through a data set before the result is achieved. Therefore, a computational form of the Pearson correlation exists (see Eq. 22), which allows to calculate the coefficient with only one pass through the data set.

$$r_{x,y} = \frac{\sum_{i=1}^{n} x_i y_i - \frac{1}{n}\left(\sum_{i=1}^{n} x_i\right)\left(\sum_{i=1}^{n} y_i\right)}{\left[\sum_{i=1}^{n} x_i^2 - \frac{1}{n}\left(\sum_{i=1}^{n} x_i\right)^2\right]^{1/2}\left[\sum_{i=1}^{n} y_i^2 - \frac{1}{n}\left(\sum_{i=1}^{n} y_i\right)^2\right]^{1/2}}, \tag{22}$$

A robust and resistant alternative to the Person product-moment correlation coefficient is the Spearman rank correlation coefficient, which is used in this work to calculate the correlation coefficient. The Spearman correlation gets calculated by applying Eq. 21 or. Eq. 22, but to the ranks of the data rather than to the data values themselves [Wilks, 2011].

7 Evaluation

To evaluate a model's capability to simulate dust emission, transport and emission, the simulation results need to be compared to observations. The observation data used is described in the previous chapter 6.1.
First of all, the two model configurations are compared among each other regarding the predicted values PM10 at the surface and AOD at 550nm. Afterwards, the evaluation of the model simulations with observation data is done.

7.1 Intercomparison of the model configurations

To get a feeling for the behavior of the configurations, the model simulations are compared to each other for both predicted parameters, PM10 at the surface and AOD at 550nm.
A scatterplot of PM10 values of GOCART vs. MADE configuration is shown in Fig. 7. The values are taken for each gridpoint of the cut domain (see right image Fig. 5). The left images shows all simulated PM10 concentrations while the right image shows only those below 2000 $\mu g/m^3$ for better visualization. For each of the images the scatterplot is given and additionally the distribution of the PM10 values of the respective configuration is shown in the smaller figures in the left and the bottom of the image. From the scatterplot can be seen, that the GOCART configuration leads to much higher PM10 values than the MADE configuration. The simulated values show a high correlation (0.88), indicating that they do not vary much in their behavior. As can be seen in the next sections, the higher values of the GOCART configuration are not correct and are overestimating PM10 concentrations, therefore, a BIAS correction based on Eq. 23 was made. The corrected

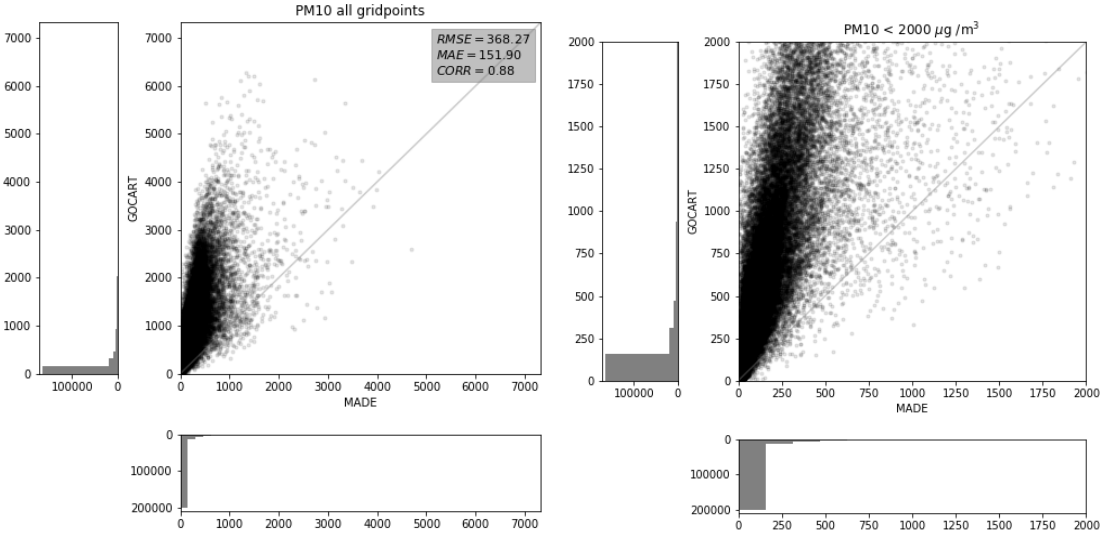

Figure 7: Comparison of simulated PM10 at surface of MADE and GOCART configuration. Left image: no size restriction, right image: only particles smaller than 2000 μg for better visualization.

version will from here on be referred to as BIAS-corrected GOCART configuration.

$$\mathrm{GOCART_{BC}} = \mathrm{GOCART} \cdot \frac{1}{T} \sum_{i=0}^{T} \frac{\mathrm{MADE}_i}{\mathrm{GOCART}_i}, \tag{23}$$

where T is the whole simulation period.
As can be seen in Fig 8, the BIAS correction reduces the difference between the model configurations for both, the RMSE (from 368.27 to 99.34 $\mu g/m^3$) and the MAE (from 151.90 to 23.43 $\mu g/m^3$). The correlation nearly remains the same (0.89).

A possible explanation for the higher values of the GOCART configuration could be the implementation of the threshold windspeed in Eq. 4, which was originally designed for the wind speed at 10m and was adapted with the friction velocity in WRF-Chem, as described in Chapter 5.1.3.1. The fact that values of 10m wind speed are usually an order of magnitude larger than the equivalent friction velocity was not considered in the implementation in WRF-Chem and could lead to a wrong emission of dust at low wind speeds. This assumption is supported by the results from Fig. 9, which show that the greatest differences can be found in the Saharan region, where the dust originates. To further confirm this thesis investigations of other parameters, e.g. wind speed or fraction velocity are needed. In addition, the difference in magnitude between friction velocity and wind speed could be taken into account by adding a conversion prior to the comparison.

For the AOD simulation a similar scatterplot can be seen in Fig.11. This parameter shows a even higher correlation between the two model configurations (0.98) but the differences are in the same magnitude when taking the values range into account (RMSE: 0.3, MAE:

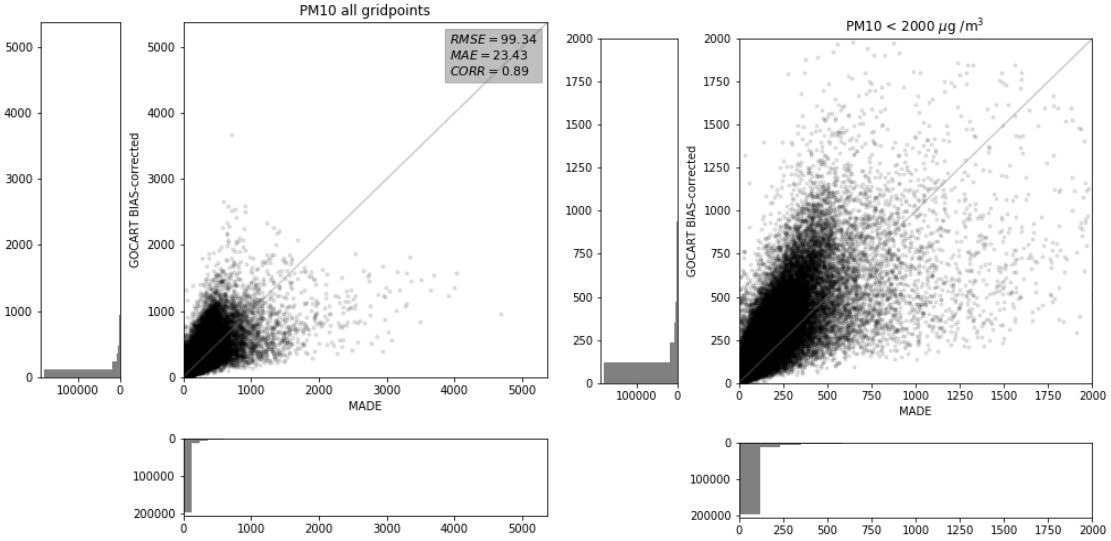

Figure 8: Comparison of simulated PM10 of MADE and BIAS-corrected GOCART configuration. Left image: no size restriction, right image: only particles smaller than 2000 μg for better visualization.

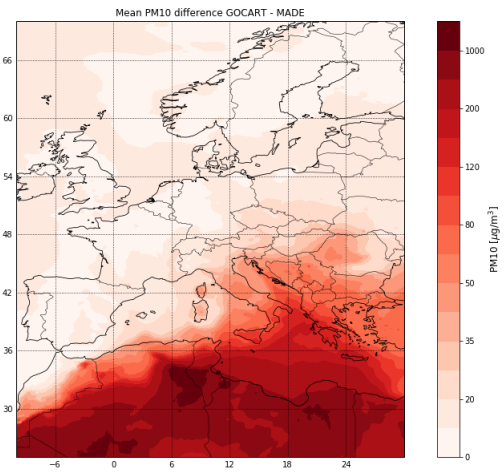

Figure 9: Mean PM10 difference between GOCART and MADE configuration over the whole simulation period.

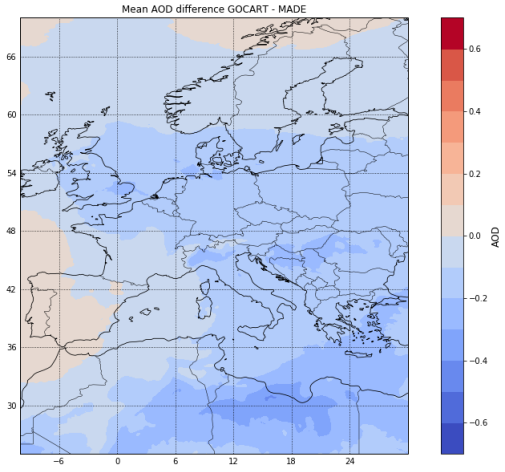

Figure 10: Mean AOD difference between GOCART and MADE configuration over the whole simulation period.

0.19). The scatterplot shows slightly higher AOD values of the MADE configuration in comparison with the GOCART configuration. This can also be seen in Fig.10 which shows the mean difference between the AOD values simulated by the GOCART and MADE con-

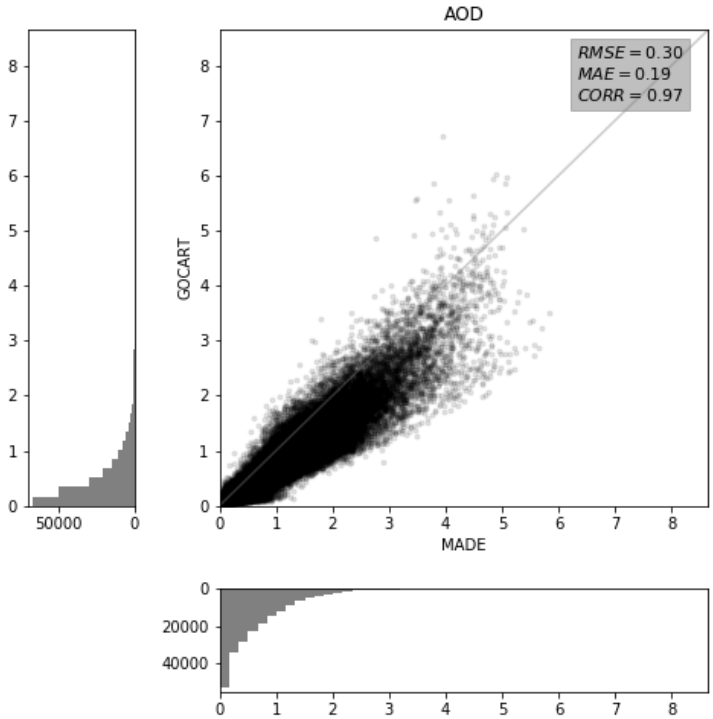

Figure 11: Comparison of simulated AOD of MADE and GOCART configuration.

figuration over the model domain. The negative (blue) values show areas where MADE simulated higher AOD values than GOCART. These areas are wide spread over the domain. The maximum lies over the Saharan region but is not as distinct as in Fig. 9 for the mean PM10 difference.
Its difficult to explain the reason for this difference without having any information about the other simulated aerosol species. To investigate this phenomenon an evaluation regarding the influencing parameters must be done.

7.2 Comparison of the interpolation techniques

Two different approaches were tested in this thesis to interpolate the simulation data for the model grid to the coordinates of the observation sites. Once, the interpolation is done with the python function **griddata** from the package **scipy.interpolate** and secondly, a nearest gridpoint approximation is made using the Haversine formular, see 6.2.1.
To evaluate the effect the MADE and the GOCART PM10 simulations were interpolated with both methods to the PM10 observation sites listed in 3. The computational expensive interpolation with **griddata** does not show significant difference to the nearest gridpoint approach, with a RMSE of 2.3 $\mu g/m^3$ (MADE) and 7.17 $\mu g/m^3$ (GOCART) and correlation coefficients of 0.99 (MADE) 0.998 (GOCART). Therefore, the simpler version is used for the further evaluation.

7.3 Comparison of model simulations with observation

7.3.1 Particular Matter (PM) - Concentration

The statistical evaluation for all EEA - observation stations and the sites on Crete is summarized in Tbl. 5 in the Appendix. The GOCART configuration shows a mean RMSE of 115.6 $\mu g/m^3$, by using the BIAS correction the error can be reduced to 58.8 $\mu g/m^3$. The MADE configuration has a mean RMSE of 44.2 $\mu g/m^3$. These high values can be explained by the character of the RMSE, penalizing large differences. For PM10 concentrations, which have an extreme event characteristic, i.e. most of the time small values with rare high outliers, the RMSE is not the appropriate choice, because the outlying high values skew the results. Therefore, the MAE is a more reliable error measurement. It shows smaller errors than the RMSE: MADE - 12.8 $\mu g/m^3$, GOCART: 53.8 $\mu g/m^3$ and BIAS - corrected GOCART configuration 12.2 $\mu g/m^3$. The BIAS correction reduces the error significantly so that it becomes comparable with the MADE configuration. The correlation with the observations is nearly the same between the model configurations (GOCART with and without BIAS correction: 0.29 and MADE: 0.32) indicating that the major difference lies in the magnitude of the values. To investigate this thesis the timeseries of four sites are examined. To picture and investigate characteristics of different emission source and location of observation site a fitting selection was made (rural - background: MT0007, traffic - urban: MK0038A, industrial - suburban: MK0045A) and a station of Crete, Finokalia.

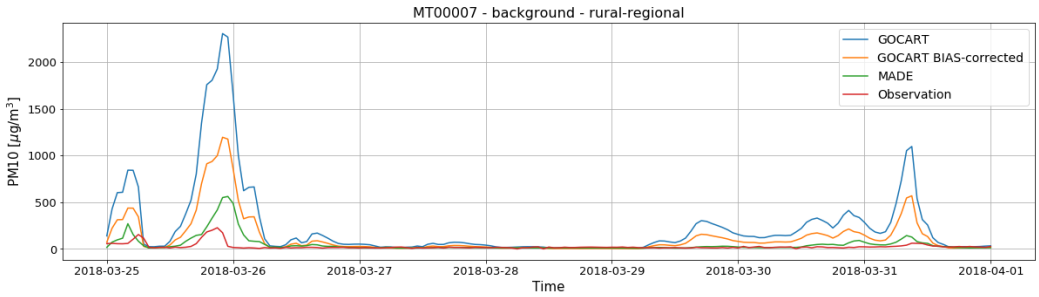

(a) Background - rural

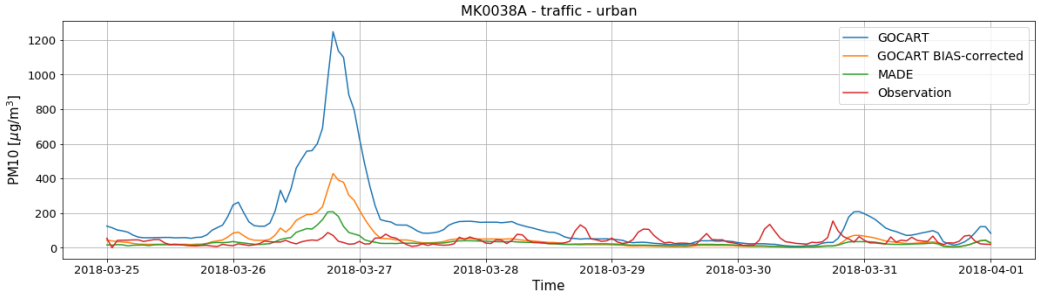

(b) Traffic - urban

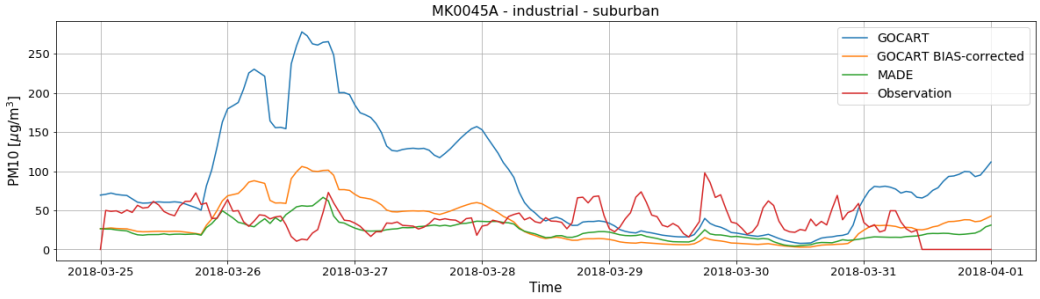

(c) Industrial - suburban

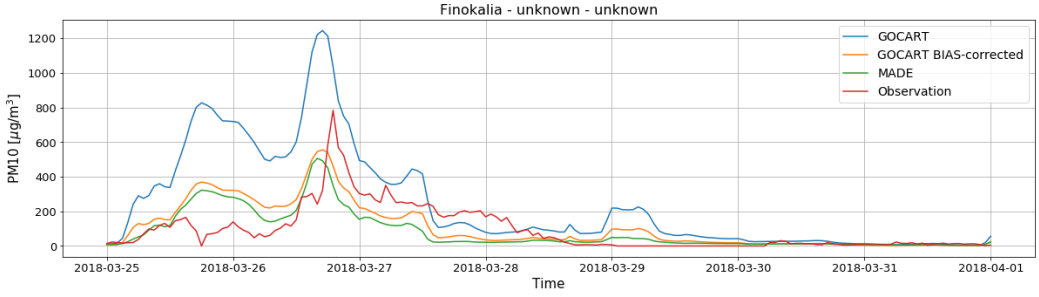

(d) Crete

Figure 12: Timeseries of PM10 concentrations for selected observation station with different predominant emission sources and one of the Crete sites. Observations in red, MADE configuration in green, GOCART configuration in blue and the BIAS corrected GOCART configuration in orange.

For a better visualization a smaller time period (3/25/2018 00UTC - 4/1/2018 00UTC) than the evaluation periode (3/22/2018 00UTC - 4/14/2018 23UTC) is shown. The results can be seen in Fig. 12 a) - d). The major difference between the model configuration lies indeed in the level of the values as their behavior does not differ much. The GOCART configuration overestimates the PM10 concentration for all presented observation stations, while the BIAS corrected version as intended shows similar magnitudes as the MADE configuration. The pattern of the PM10 observations is well represented by the simulations especially for the background-rural site (a) and Finokalia (d). It can be seen that the observations for the traffic and industrial stations are overlaid with disturbances probability from anthropogenic sources. Therefore the results of background stations and these on Crete are more trustworthy for verification than those with traffic or industries as predominant emission source. The sites on Crete recorded a high peak of PM10 with the strongest Saharan dust outbreak on 3/22/2018 (Finokalia at 17UTC 5380 μg/m^3, Iraklion at 14UTC 4262 μg/m^3) which was not simulated in any model with the same intensity, even though both simulated a peak (GOCART: Finokalia at 19UTC 1632 μg/m^3, Iraklion at 15UTC 2644 μg/m^3; MADE: Finokalia at 14UTC 574 μg/m^3, Iraklion at 15UTC 1229 μg/m^3). This huge difference leads to especially high RMSE and MAE for these two sites in the evaluation, as can be seen in Tbl. 5 . Altogether the overestimation of the GOCART configuration can be seen, with much higher RMSE and MAE values for all examples. The BIAS corrected version reduces the errors accordingly, resulting in similar, slightly higher values than the MADE configuration.

To investigate the simulated PM10 concentrations further all observation stations are sorted under consideration of their predominant emission source and location. The error measurements are averaged and can be found in Tbl. 6. To visualize the found results scatterplots similar to those in the model comparison section are made again for the four different predominant emission types (background (Fig. 14), industrial (Fig. 15) and traf-

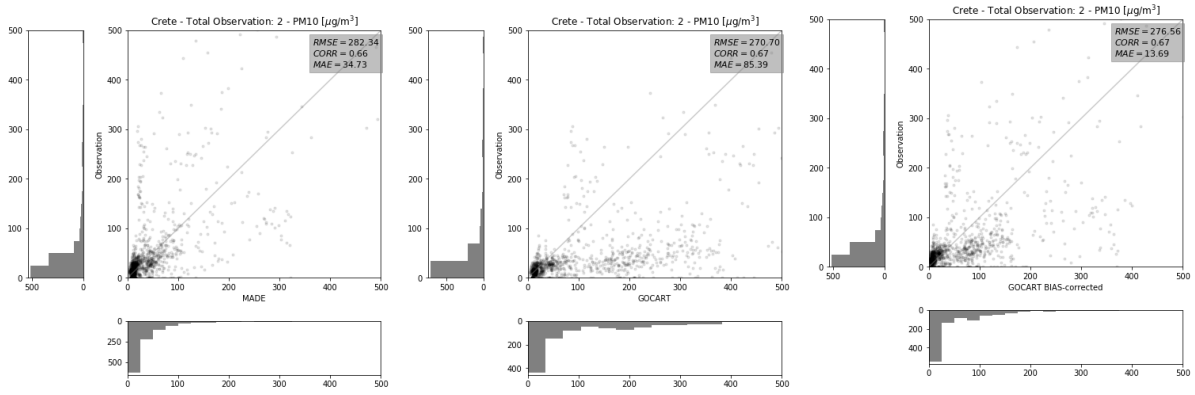

(a) MADE (b) GOCART (c) BIAS - corrected GOCART

Figure 13: Comparison of PM10 simulations for all observation sites on Crete with MADE, GOCART and BIAS - corrected GOCART configuration (from left to right).

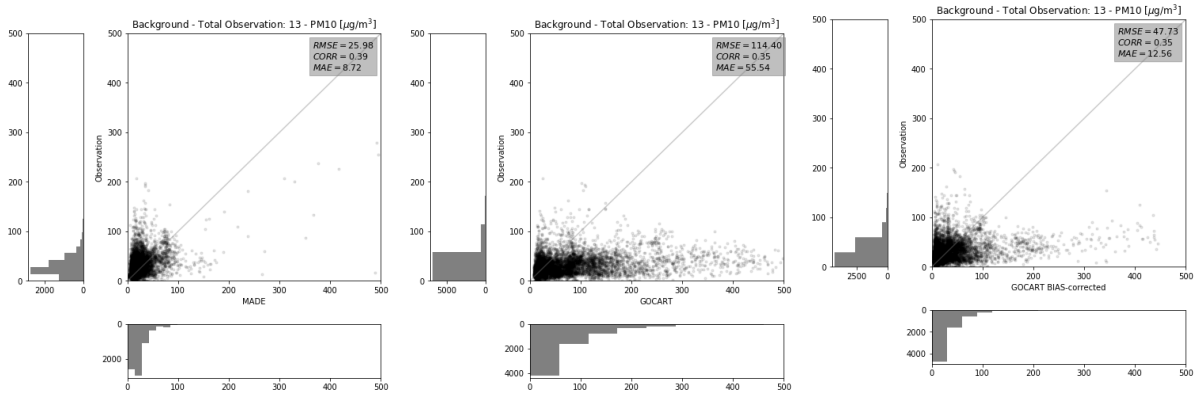

(a) MADE (b) GOCART (c) BIAS - corrected GOCART

Figure 14: Comparison of PM10 simulations for all background observation sites with MADE, GOCART and BIAS - corrected GOCART configuration (from left to right).

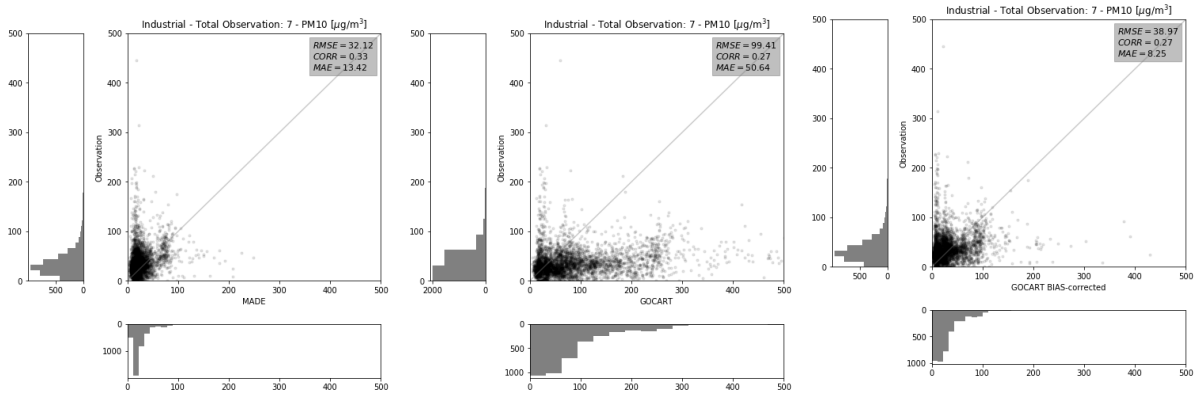

(a) MADE (b) GOCART (c) BIAS - corrected GOCART

Figure 15: Comparison of PM10 simulations for all industrial observation sites with MADE, GOCART and BIAS - corrected GOCART configuration (from left to right).

fic (Fig. 16)) and the locations (rural-regional (Fig. 17), urban (Fig. 18) and suburban (Fig. 19)) as well as the sites on Crete (Fig. 13).
Starting with the results for Crete, you can see that the GOCART configuration clearly overestimates the observed PM10 concentrations. The BIAS correction reduces this problem, in comparison with the MADE configuration, however, it mostly still overestimates PM10. Furthermore, it can be seen that the MADE configuration shows better performance than the other two configurations when comparing the distributions. The RMSE and MAE values appear to be higher for the MADE configuration which is due to high peak in the observations which is underestimated in the simulations most of the MADE configuration. When taking a closer look on the evaluations regarding predominant emission type and location, it can be seen that the MADE configuration shows better results

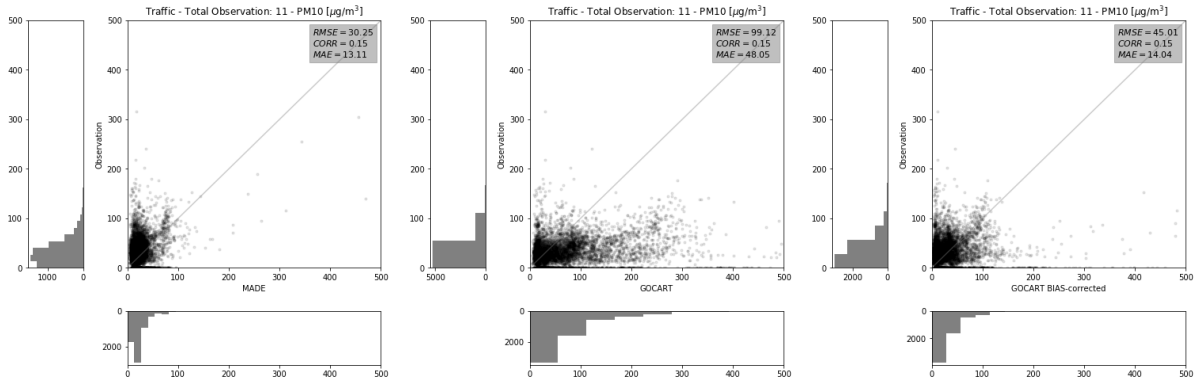

(a) MADE (b) GOCART (c) BIAS - corrected GOCART

Figure 16: Comparison of PM10 simulations for all traffic observation sites with MADE, GOCART and BIAS - corrected GOCART configuration (from left to right).

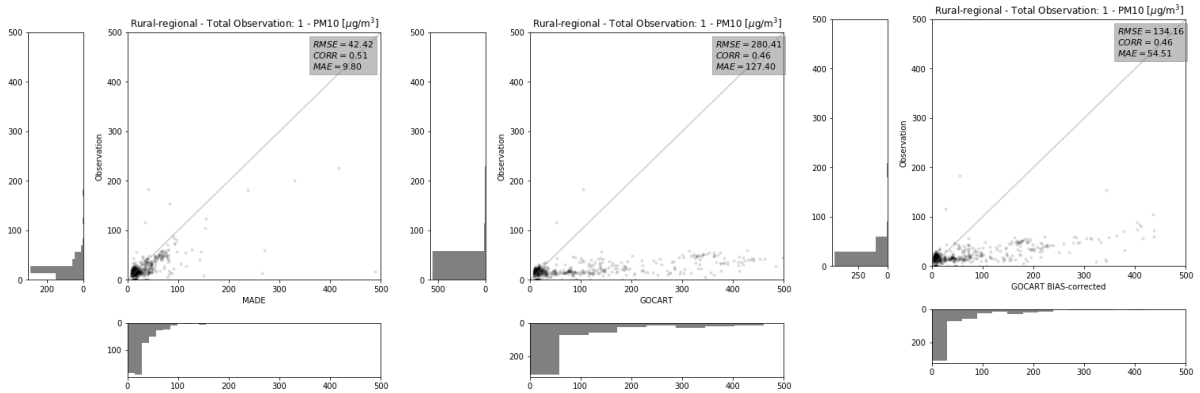

(a) MADE (b) GOCART (c) BIAS - corrected GOCART

Figure 17: Comparison of PM10 simulations for all rural-regional observation sites with MADE, GOCART and BIAS - corrected GOCART configuration (from left to right).

than the GOCART configuration as well as the BIAS corrected GOCART version for both RMSE and MAE. Furthermore, it can be seen that the distributions of the simulations fit those of the observations better for sites with background predominant emission source than for those with traffic or industrial emissions. The correlation coefficient is rather low for all three categories and has its lowest values for traffic sites with 0.15 for all model configurations. Eventually there is a similar amount of observation for all three predominant emission categories. This is not the case for the location categories. Only one site is classified as rural-regional, followed by four sites for suburban, all others are urban stations. Hence, the results should be interpreted with caution. The rural-regional observation site is well represented by the MADE configuration and highly overestimated by the GOCART configuration as well as the BIAS corrected version. This can also be seen for the other location categories. The MADE configuration shows similar distributions to those of the

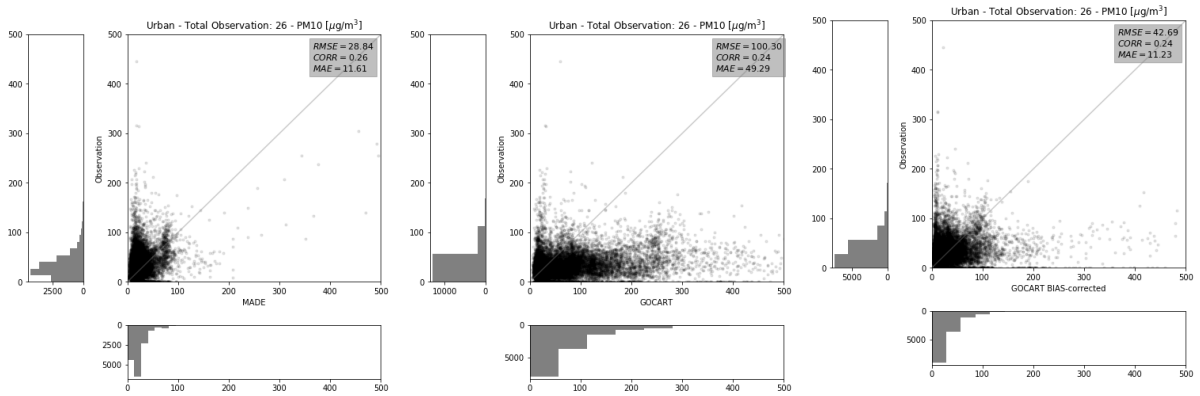

(a) MADE (b) GOCART (c) BIAS - corrected GOCART

Figure 18: Comparison of PM10 simulations for all urban observation sites with MADE, GOCART and BIAS - corrected GOCART configuration (from left to right).

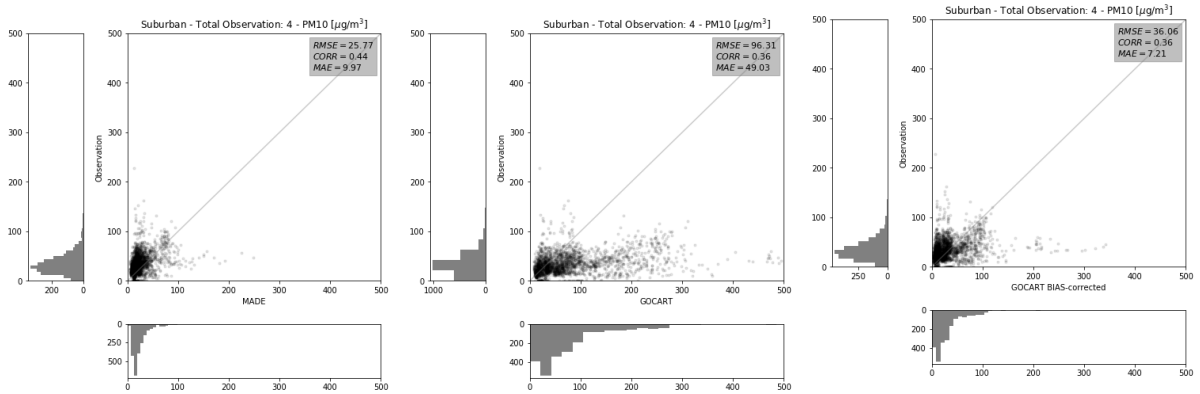

(a) MADE (b) GOCART (c) BIAS - corrected GOCART

Figure 19: Comparison of PM10 simulations for all suburban observation sites with MADE, GOCART and BIAS - corrected GOCART configuration (from left to right).

observation than the GOCART configurations, indicating an overall better representation of the PM10 concentrations by the MADE configuration although a simple BIAS correction improves the outcome of the GOCART configuration.

7.3.2 Aerosol Optical Depth (AOD)

In WRF-Chem the aerosol optical properties are calculated for wavelengths of 300, 400, 600 and 999 nm following [Barnard et al., 2010]. A spherical shell/core configuration is used to calculate the bulk refractive index of the particles in a bin. This index is needed to determine the absorption and scattering efficiency as well as the asymmetry parameter for each bin by using the shell/core Mie theory ([Ackerman and Toon, 1981]). A spherical shell/core configuration was chosen, where all species except black carbon are uniformly distributed within a shell that surrounds a core consisting only of black carbon [Barnard et al., 2010]. In order to derive the model AOD at 550 nm, the Ångström power law is used:

$$AOD(550) = AOD(400) \cdot \left(\frac{550}{400}\right)^{\alpha} \tag{24}$$

where α is the Ångström exponent calculated with $\alpha = \frac{ln\left(\frac{AOD(400)}{AOD(600)}\right)}{ln\left(\frac{600}{400}\right)}$. This approach is consistent with the WRF-Chem framework as these equations are also applied for the conversion of AOD for further use in aerosol-radiation interaction [Kumar et al., 2014].
For evaluating AOD simulations first of all a case study has been chosen. Athens is the only site for which all three observation types (AERONET, EARLINET and MODIS) are available. The results are shown in Fig. 20. EARLINET measurements are shown as black dots and as can be seen only three measurements are available for the whole evaluation period. It can be found that the values retrieved of EARLINET measurements are higher than of the other observations, but a further evaluation is not possible and significant. AERONET and MODIS observations show a lot of missing values but enough to make a verification. As noticed in the model intercomparison chapter the MADE configuration shows a similar pattern and behavior but simulates higher AOD values than the GOCART setting. The difference, however, is not as big as that of the PM10 evaluation.
The simulated high peaks of AOD as seen in Fig. 20 cannot be found in this intensity in the observations but an increase can be seen. AERONET shows higher values than the MODIS observations and even than the WRF-Chem simulations sometimes. The MODIS measurements mostly are similar but occasionally much lower than the simulations.
The results of the statistical evaluation for the three stations Athens, Finokalia and Lampedusa for which AERONET data was available can be found in Tbl. 7 in the Appendix. For Lampedusa the interpolation of MODIS did not deliver a result, therefore, no evaluation was possible and for Finokalia only one measurement of MODIS was found, hence, no correlation coefficient could be calculated.
The model configurations show similar correlations for both AERONET and MODIS, with a much lower correlation coefficient for MODIS data of only 0.18/0.21 (MADE/GOCART). The correlation coefficient for AERONET data is rather good, around 0.80 for both configurations. The MADE configuration shows higher RMSE and MAE values for all observation sources and sites than with GOCART. The same can be seen for the AERONET data. On the basis of the similar correlation it can be assumed that the lower AOD values of the GOCART configuration represent the available observations better and are leading to

lower RMSE and MAE.
To estimate the AOD simulations further the MODIS observations were interpolated to the coordinates of the previous PM10 observation sites for comparison. The results can be seen in Tbl. 4 in the Appendix. It can be found that the number of available measurements per station varies from only one measurement to 20 for the whole validation period. It can be seen that the correlation coefficient is similar for both model configurations and quite good (around 0.8 for most of the sites). The previous findings are validated as for AERONET, the MADE configuration yields higher scores than the GOCART configuration.
It can hardly be decided whether the lower values of the GOCART configuration show the reality better than the slightly higher values of the MADE configuration or if there is just a lack of the amount of measurements to represent the actual conditions correctly. Especially for EARLINET and AERONET data it is not possible to make a conclusion because of the missing data and low availability.

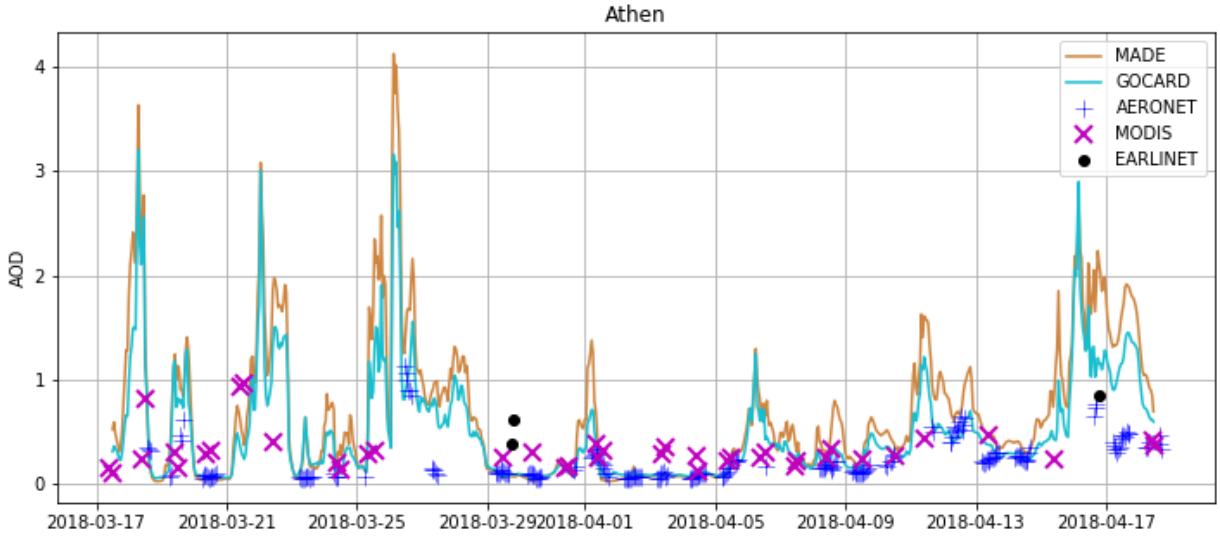

Figure 20: AOD observations from AERONET (blue), EARLINET (black) and MODIS (magenta) and AOD simulation of MADE (orange) and GOCART (cyan) configuration over the whole periode for Athens.

8 Conclusions and future scope

The goal of this thesis is the evaluation of a Saharan dust episode simulated with the WRF-Chem model investigating two different settings.
By comparing the two configurations it can be seen that the GOCART setting simulated much higher PM10 concentrations as the MADE configuration. The simulations do not vary much regarding the pattern of the PM10 concentrations but regarding their magnitude. The major difference can be found over the desert areas, where the emission schemes yield very different values. When compared to observation data it can be found, that the GOCART configuration clearly overestimates PM10 concentrations, while the MADE configuration is closer to the actual values.

The conspicuous overestimation of the GOCART configuration can be traced back to implementation of the GOCART dust emission scheme into the WRF code. In the WRF-Chem GOCART dust emission scheme the threshold wind speed required for initiating erosion is derived in terms of friction velocity, while in the the original GOCART scheme 10m wind is used to determine the threshold. Values of the friction velocity are usually an order of magnitude smaller than the equivalent 10m wind speed, which was not considered in the implementation into the WRF code. Therefore, emissions are not set to zero until wind speeds are below a very low threshold magnitude. The major difference in emission source regions could be due to the false treatment of dust lifting at low wind speeds.
A simple BIAS correction has been made to investigate the impact on the results of the GOCART simulation. It could be found that this approach improves the outcome of the simulation extremely, leading to results comparable to those of MADE which is a far more complex model and needs more computational resources.
To investigate the PM10 simulations further it would be interesting to look at different atmospheric parameters like wind speed or a planetary boundary layer parameter like friction velocity or planetary boundary height. This would allow to draw conclusions regarding the hypothesis of the false lifting of dust at low wind speeds. In the following a conversion from friction velocity to 10m wind speed could be done for the threshold wind speed.
To test the BIAS corrected version of GOCART the same correction could be applied to another independent case study. If the same improvement can be observed, the BIAS correction could be considered a suitable option to improve the quality of the GOCART configuration PM10 simulation in a simple way.

The simulated AOD values of the MADE configuration are slightly higher than those of the GOCART setting but the difference is not as major as that for PM10. The pattern of the AOD values is similar of both model configurations. When comparing to Earth observation data the in previous studies found overestimation of AOD could not be confirmed. Two of a total of three EARLINET measurements showed higher AOD values than the models simulated but the number of observations is not sufficient enough for a conclusion regarding over- or underestimation. For AERONET and MODIS data is can be seen that the AOD peaks are overestimated by the models and the background AOD, hence, where no major dust outbreak happened, is slightly underestimated for AERONET data and of

a similar magnitude for MODIS data.
Unfortunately, the available observation data shows a lot of missing values which can have a major influence on the evaluation. Therefore, a longer simulation period or more case studies would be necessary to make sufficient statements.
For the comparison between the model runs it can be seen that a clear pattern for the major difference like the desert area for PM10 could not be found for AOD. Hence, a suggestion where the major difference between the models comes from cannot be traced back. Additionally, not only dust particles lead to extinction of radiation in the atmosphere. Many atmospheric constituents, like different chemical species or black carbon contribute to the total AOD. Therefore, a set of other parameters like concentrations of specific gas molecules, ect. would be necessary to determine where the difference between the model configurations arises.
For the MODIS data a regridding could be considered to evaluate the model over a large area and not only of specific points. This would also only make sense if the observation period is large enough to have a sufficient dataset where the missing data due to cloud-clearing and other post-processing processes are of no consequence.

Both the GOCART and the MADE configuration are capable to represent the pattern on PM10 concentration and AOD sufficiently. The MADE configuration performs better in terms of magnitude of the values for PM10 whereas for AOD the simulated values do not differ much regarding their magnitude. A simple BIAS correction improves the simulated values of the GOCART configuration.

9 Acknowledgements

First of all, I would like to thank my thesis advisor ao. Univ.-Prof. Mag. Dr. Leopold Haimberger of the Department of Meteorology and Geophysics at the University of Vienna. The door to Prof. Haimbergers office was always open whenever I ran into a trouble spot or had a question about my research or writing and he steered me in the right direction whenever I needed it.
I would also like to thank the experts of the ZAMG who provided me with the model simulations and some of the observation datasets for this research project: Mag. Marcus Hirtl, Mag. Claudia Flandorfer and MMMag. Dr. Barbara Scherllin-Pirscher. Without their passionate participation and input, this master thesis would not have been possible. I would like to thank the ZAMG for running the WRF model and make EEA and MODIS datasets available.
The research leading to these results has received funding from the European Union's Horizon 2020 research and innovation programme under grant agreement No 654109 and previously from the European Union Seventh Framework Programme (FP7/2007-2013) under grant agreement n° 262254. I acknowledge EARLINET for providing aerosol LIDAR profiles available at https://data.earlinet.org/.
We thank the Principal Investigators Vassilis Amiridis, Nikolaos Mihalopoulos and Daniela Meloni for their effort in establishing and maintaining ATHENS-NOA, Finokalia-FKL and Lampedusa sites.
Finally, I must express my very profound gratitude to my parents and to my grandparents for providing me with unfailing support and continuous encouragement throughout my years of study and through the process of researching and writing this thesis. My special thanks go to MMag. Renate Thumb for providing me her photo of the Saharan dust storm at the airport of Iraklion, my sister for her motivational speeches throughout the years and Dr. Klaus-Jürgen Bertram for his efforts to proofread this thesis. This accomplishment would not have been possible without them. Thank you.

10 Appendix

AOD MODIS		RMSE		MAE		CORR	
Name	# OBS	MADE	GOCART	MADE	GOCART	MADE	GOCART
BG0018A	13	0.29	0.16	0.23	0.13	0.90	0.90
BG0019A	17	0.28	0.17	0.23	0.14	0.58	0.70
BG0038A	13	0.21	0.12	0.17	0.09	0.65	0.65
BG0040A	17	0.25	0.15	0.20	0.13	0.67	0.72
BG0050A	12	0.25	0.15	0.21	0.13	0.84	0.86
BG0057A	15	0.26	0.14	0.22	0.13	0.68	0.81
BG0058A	6	0.39	0.22	0.30	0.18	0.49	0.49
BG0066A	16	0.21	0.12	0.19	0.11	0.98	0.96
BG0073A	11	0.22	0.13	0.18	0.11	0.81	0.79
IT0898A	1	1.03	0.65	1.03	0.65	-	-
IT0934A	8	0.18	0.10	0.09	0.06	0.55	0.55
IT1491A	1	1.03	0.65	1.03	0.65	-	-
MK0030A	13	0.42	0.24	0.28	0.17	0.83	0.80
MK0031A	13	0.41	0.23	0.28	0.16	0.82	0.79
MK0034A	15	0.41	0.29	0.28	0.19	0.81	0.77
MK0035A	4	0.40	0.23	0.36	0.21	0.80	0.80
MK0036A	20	0.43	0.29	0.25	0.17	0.79	0.79
MK0037A	10	0.46	0.30	0.30	0.19	0.88	0.91
MK0038A	11	0.45	0.29	0.28	0.17	0.81	0.85
MK0040A	14	0.38	0.21	0.25	0.14	0.60	0.71
MK0041A	1	0.24	0.10	0.24	0.10	-	-
MK0043A	13	0.41	0.23	0.28	0.17	0.82	0.79
MK0044A	19	0.31	0.16	0.20	0.12	0.80	0.76
MK0045A	18	0.35	0.20	0.21	0.13	0.78	0.76
MK0048A	13	0.38	0.21	0.25	0.15	0.88	0.82
RS0032A	3	0.69	0.40	0.51	0.30	0.50	-0.50
Finokalia	1	0.48	0.21	0.48	0.21	-	-

Table 4: Statistics (RMSE, MAE and Correlation) for MADE and GOCART configuration with MODIS AOD observation interpolated to the coordinates of the PM10 observation stations.

PM10 [$\mu g/m^3$]	RMSE			MAE			Correlation		
	MADE	GOCART	GOCART BC	MADE	GOCART	GOCART BC	MADE	GOCART	GOCART BC
BG0018A	17.17	110.87	36.84	4.96	51.16	4.39	0.47	0.47	0.47
BG0019A	28.50	49.11	29.21	21.69	16.26	15.87	0.20	0.20	0.20
BG0038A	22.96	72.75	34.11	8.15	28.08	0.98	0.38	0.35	0.35
BG0040A	27.64	85.63	35.01	5.09	48.19	1.61	0.21	0.10	0.10
BG0044A	28.10	86.32	36.37	13.48	30.64	6.38	0.51	0.35	0.35
BG0050A	21.26	82.76	29.23	4.65	48.63	2.04	0.33	0.17	0.17
BG0057A	33.51	53.09	32.68	23.23	16.14	17.83	0.38	0.57	0.57
BG0058A	22.44	130.98	46.30	1.89	69.34	11.12	0.39	0.36	0.36
BG0066A	17.12	56.81	19.67	8.13	33.38	2.87	0.24	0.42	0.42
BG0071A	24.12	79.68	33.23	9.26	32.40	1.95	0.53	0.24	0.24
BG0073A	20.39	78.86	26.58	7.96	45.33	1.26	0.33	0.23	0.23
IT0898A	23.42	59.57	33.94	0.62	29.85	6.71	-0.11	-0.07	-0.07
IT0934A	22.79	63.44	34.68	1.66	33.69	9.60	-0.02	-0.01	-0.01
IT1491A	25.60	59.68	35.37	2.93	27.54	4.50	-0.14	-0.10	-0.10
MK0030A	26.15	84.19	30.55	12.75	49.38	6.46	0.46	0.39	0.39
MK0031A	31.83	87.81	36.41	13.63	48.50	7.37	0.35	0.24	0.24
MK0034A	21.66	101.01	32.95	8.94	55.80	0.54	0.38	0.37	0.37
MK0035A	27.76	98.22	29.83	11.22	58.42	2.44	0.29	0.39	0.39
MK0036A	47.68	87.65	50.58	24.13	32.64	17.14	0.20	0.09	0.09
MK0037A	24.53	152.32	44.87	5.65	88.51	13.94	0.43	0.38	0.38
MK0038A	30.41	144.60	46.41	11.12	71.74	2.83	0.41	0.40	0.40
MK0040A	39.41	86.36	41.83	21.70	38.98	14.16	0.23	0.17	0.17
MK0041A	37.08	83.09	34.46	25.10	39.85	16.52	0.30	0.39	0.39
MK0043A	41.77	78.53	42.73	28.61	33.53	22.35	0.37	0.28	0.28
MK0044A	38.55	99.81	43.69	14.07	49.02	5.60	0.15	0.13	0.13
MK0045A	26.40	83.74	31.02	11.75	46.75	4.85	0.40	0.33	0.33
MK0048A	26.98	82.46	30.00	15.61	45.92	8.47	0.40	0.33	0.33
MT00004	33.36	291.52	127.53	2.96	32.61	49.61	0.38	0.40	0.40
MT00005	41.78	286.04	136.97	13.85	135.97	59.84	-0.32	-0.22	-0.22
MT00007	42.42	280.41	134.16	9.80	127.40	54.51	0.51	0.46	0.46
RS0032A	22.65	76.10	31.15	6.82	39.33	1.42	0.41	0.31	0.31
Finokalia	283.83	286.46	274.22	23.70	86.97	3.33	0.67	0.68	0.68
Iraklio	280.85	254.94	278.89	45.77	83.81	24.05	0.64	0.66	0.66

Table 5: Statistics (RMSE, MAE and Correlation) for the configuration MADE,GOCART and GOCART BIAS-corrected (GOCART BC) with EEA PM10 observations for each observation station

PM10	RMSE			MAE			Correlation		
predominant emission									
	MADE	GOCART	GOCART BC	MADE	GOCART	GOCART BC	MADE	GOCART	GOCART BC
background	25.98	114.40	47.73	8.72	55.54	12.56	0.39	0.35	0.35
industrial	32.12	99.41	38.97	13.42	50.64	8.25	0.33	0.27	0.27
traffic	30.25	99.12	45.01	13.11	48.05	14.04	0.15	0.15	0.15
Crete	282.34	270.70	276.56	34.73	85.39	13.69	0.66	0.67	0.67
location									
	MADE	GOCART	GOCART BC	MADE	GOCART	GOCART BC	MADE	GOCART	GOCART BC
rural-regional	42.42	280.41	134.16	9.80	127.40	54.51	0.51	0.46	0.46
suburban	25.77	96.31	36.06	9.97	49.03	7.21	0.44	0.36	0.36
urban	28.84	100.30	42.69	11.61	49.29	11.23	0.26	0.24	0.24
Crete	282.34	270.70	134.16	34.73	85.39	13.69	0.66	0.67	0.67

Table 6: Statistics (RMSE, MAE and Correlation) for the configuration MADE,GOCART and GOCART BIAS-corrected (GOCART BC) with EEA PM10 observations, evaluated according to the observation station attributes location and predominant emission. The catagory unknown represents the two stations Finokalia, GR and Iraklio, GR.

	RMSE		MAE		Correlation	
AERONET						
	MADE	GOCART	MADE	GOCART	MADE	GOCART
Athen	0.43	0.25	0.23	0.11	0.77	0.75
Finokalia	0.63	0.39	0.33	0.11	0.85	0.85
Lampedusa	0.78	0.60	0.37	0.23	0.85	0.83
MODIS						
	MADE	GOCART	MADE	GOCART	MADE	GOCART
Athen	0.69	0.51	0.28	0.13	0.18	0.21
Finokalia	0.48	0.21	0.48	0.21	-	-

Table 7: Statistics (RMSE, MAE and Correlation) for the MADE and GOCART configuration with AERONET and MODIS AOD observations. There are no MODIS observations over the whole period after interpolation for Lampedusa and only one measurement for Finokalia.

References

[Ackerman and Toon, 1981] Ackerman, T. P. and Toon, O. B. (1981). Absorption of visible radiation in atmosphere containing mixtures of absorbing and nonabsorbing particles. *Appl. Opt.*, 20.

[Ackermann et al., 1998] Ackermann, I. J., Hass, H., Memmesheimer, M., Ebel, A., Binkowski, F. S., and Shankar, U. (1998). Modal aerosol dynamics model for Europe: development and first applications. *Atmospheric Environment 32*.

[Alpert and Ziv, 1989] Alpert, P. and Ziv, B. (1989). The Sharav Cyclone: Observations and some theoretical considerations. *Journal of Geophysical Research: Atmospheres*, 94.

[Barnard et al., 2010] Barnard, J., Fast, J., G., P.-M., Arnott, W., and Laskin, A. (2010). Technical Note: Evaluation of the WRF-Chem "Aerosol Chemical to Aerosol Optical Properties" Module using data from the MILAGRO campaign. *Atmospheric Chemistry and Physics*, 10.

[Benedetti et al., 2013] Benedetti et al. (2013). Mineral Dust - A Key Player in the Earth System; Chapter 10 - Numerical Prediction of Dust. `https://ntrs.nasa.gov/search.jsp?R=20140012667`.

[Binkowski and Shankar, 1995] Binkowski, F. S. and Shankar, U. (1995). The regional particulate matter model, 1. mode desription and preliminary results. *Journal of Geophysical research 100*.

[Bou Karam et al., 2010] Bou Karam, D., Flamant, C., Cuesta, J., Pelon, J., and Williams, E. (2010). Dust emission and transport associated with a Saharan depression: February 2007 case. *Journal of Geophysical Research*, 115.

[Chen and Dudhia, 2011] Chen, F. and Dudhia, J. (2011). Coupling an advanced land surface-hydrology model with the Penn State-NCAR MM5 modeling system. Part I: model implementation and sensitivity. *Monthly Weather Review*, 129.

[Chin et al., 2000] Chin, M., Savoie, D. L., Huebert, B. J., Bandy, A. R., Thornton, D. C., Bates, T. S., Quinn, P. K., Saltzman, E. S., and De Bruyn, W. J. (2000). Atmospheric sulfur cycle simulated in the global model GOCART: Comparison with field observations and regional budgets. *Journal of Geophysical Research 105*.

[Ciamprone et al., 2019] Ciamprone, S., Mona, L., and DÁmico, G. (2019). EARLINET Level 3 Algorithm Theoretical Basis Document. *Aerosol, Clouds and Trace Gases Research Infrastructure*.

[DWD, 2020] DWD (06.04.2020). Aerosols). `https://www.dwd.de/EN/research/observing_atmosphere/composition_atmosphere/aerosol/aerosol_node.html`.

[EARLINET homepage, 2019] EARLINET homepage (06.12.2019). https://www.earlinet.org/index.php?id=earlinet_homepage.

[Eltahan et al., 2018] Eltahan, M., Shokr, M., and O.sherif, A. (2018). Simulation of Severe Dust Events over Egypt Using Tuned Dust Schemes in Weather Research Forecast (WRF-Chem). *Atmosphere*, 9.

[European Environment Agency, 2019] European Environment Agency (2019). Air quality in Europe - 2019 report. *EEA Report*, 10.

[Giles et al., 2018] Giles, D., Sinyuk, A., Sorokin, M., Schafer, J., Smirnov, A., Slutsker, I., Eck, T., Holben, B., Lewis, J., Campbell, J., Welton, E., Korkin, S., and Lyapustin, A. (2018). Advancements in the Aerosol Robotic Network (AERONET) Version 3 database â€“ automated near-real-time quality control algorithm with improved cloud screening for Sun photometer aerosol optical depth (AOD) measurements . *Atmospheric Measurement Techniques Discussions*.

[Ginoux et al., 2001] Ginoux, P., Chin, M., Tegen, I., Prospero, J. M., Holben, B., Dubovik, O., and Lin, S.-J. (2001). Sources and distributions of dust aerosols simulated with the gocart model. *Journal of Geophysical Research: Atmospheres*, 106.

[Goudie, 2006] Goudie, A. S. (2006). *Desert dust in the global system : 41 tables*. Springer.

[Grell and Freitas, 2013] Grell, G. and Freitas, S. (2013). A scale and aerosol aware stochastic convective parameterization for weather and air quality modeling. *Atmos. Chem. Phys. Discuss.*, 13.

[Grell et al., 2005] Grell, G. A., Peckham, S. E., Schmitz, R., McKeen, S. A., Frost, G., Skamarock, W. C., and Eder, B. (2005). Fully coupled "online" chemistry within the WRF model. *Atmospheric Environment*.

[Guenther et al., 2006] Guenther, A., Karl, T., Harley, P., Wiedinmyer, C., Palmer, P. I., and Geron, C. (2006). Estimates of global terrestrial isoprene emissions using megan (model of emissions of gases and aerosols from nature). *Atmospheric Chemistry and Physics*, 6(11).

[Heintzenberg, 1994] Heintzenberg, J. (1994). The life cycle of the atmospheric aersol. *Topics in atmospheric and interstellar physics and chemistry 251-270*.

[Hendricks et al., 2012] Hendricks, J., Righi, M., and Aquila, V. (2012). Global Atmospheric Aerosol Modeling. https://ntrs.nasa.gov/search.jsp?R=20120011689.

[Holben et al., 1998] Holben, B., Eck, T., Slutsker, I., TanrÃ©, D., Buis, J., Setzer, A., Vermote, E., Reagan, J., Kaufman, Y., Nakajima, T., Lavenu, F., Jankowiak, I., and Smirnov, A. (1998). AERONETâ€"A Federated Instrument Network and Data Archive for Aerosol Characterization. *Remote Sensing of Environment*, 66.

[Hsu et al., 2004] Hsu, N., Tsay, S.-C., King, M., and Herman, J. (2004). Aerosol properties over bright-reflecting source regions. *IEEE Transactions on Geoscience and Remote Sensing*, 42(3).

[Iacono et al., 2008] Iacono, M. J., Delamere, J. S., Mlawer, E. J., Shephard, M. W., Clough, S. A., and Collins, W. D. (2008). Radiative forcing by long-lived greenhouse gases: Calculations with the AER radiative transfer models. *Journal of Geophysical Research: Atmospheres*, 113.

[Kaskaoutis et al., 2019] Kaskaoutis, D., Rashki, A., Dumka, U., Mofidi, A., Kambezidis, H., Psiloglou, B., Karagiannis, D., Petrinoli, K., and Gavriil, A. (2019). Atmospheric dynamics associated with exceptionally dusty conditions over the eastern Mediterranean and Greece in March 2018. *Atmospheric Research*, 218.

[Kaufman et al., 2005] Kaufman, Y. J., Koren, I., Remer, L. A., Tanré, D., Ginoux, P., and Fan, S. (2005). Dust transport and deposition observed from the Terra Moderate Resolution Imaging Spectroradiometer (MODIS) spacecraft over the Atlantic Ocean. *Journal of Geophysical Research: Atmospheres*, 110.

[Kazil, 2009] Kazil, J. (2009). Introduction to aerosol modeling with WRF/Chem. `http://www.mce2.org/Kazil_2009_07_22_Tutorial%20%28Rainer%29.pdf`.

[Keep Talking Greece, 2020] Keep Talking Greece (24.06.2020). `https://www.keeptalkinggreece.com/2018/03/24/greece-sahara-dust-science/`.

[Kim et al., 2015] Kim, K.-H., Kabir, E., and Kabir, S. (2015). A review on the human health impact of airborne particulate matter. *Environment International*, 74.

[Kumar et al., 2014] Kumar, R., Barth, M. C., Pfister, G. G., Naja, M., and Brasseur, G. P. (2014). WRF-Chem simulations of a typical pre-monsoon dust storm in northern India: influences on aerosol optical properties and radiation budget. *Atmospheric Chemistry and Physics*, 14.

[LeGrand et al., 2019] LeGrand, S. L., Polashenski, C., Letcher, T. W., Creighton, G. A., Peckham, S. E., and Cetola, J. D. (2019). The AFWA dust emission scheme for the GOCART aerosol model in WRF-Chem v3.8.1. *Geoscientific Model Development*, 12.

[Marticorena and Bergametti, 1995] Marticorena, B. and Bergametti, G. (1995). Modeling the atmospheric dust cycle: 1. design of a soil-derived dust emission scheme. *Journal of Geophysical Research: Atmospheres*, 100.

[Möller, 2011] Möller, D. (2011). *Luft : Chemie, Physik, Biologie, Reinhaltung, Recht*. De Gruyter.

[Morrison et al., 2005] Morrison, H., Curry, J. A., and Khvorostyanov, V. I. (2005). A New Double-Moment Microphysics Parameterization for Application in Cloud and Climate Models. Part I: Description. *Journal of the Atmospheric Sciences*, 62.

[Morrison et al., 2009] Morrison, H., Thompson, G., and Tatarskii, V. (2009). Impact of Cloud Microphysics on the Development of Trailing Stratiform Precipitation in a Simulated Squall Line: Comparison of One- and Two-Moment Schemes. *Monthly Weather Review*, 137.

[Nakanishi and Niino, 2006] Nakanishi, M. and Niino, H. (2006). An Improved Mellor-Yamada Level 3 Model: Its Numerical Stability and Application to a Regional Prediction of Advection Fog. *Boundary-Layer Meteorology*, 119.

[Pappalardo et al., 2014] Pappalardo, G., Amodeo, A., Apituley, A., Comeron, A., Freudenthaler, V., Linné, H., Ansmann, A., Bösenberg, J., D'Amico, G., Mattis, I., Mona, L., Wandinger, U., Amiridis, V., Alados-Arboledas, L., Nicolae, D., and Wiegner, M. (2014). EARLINET: towards an advanced sustainable European aerosol lidar network. *Atmospheric Measurement Techniques*, 7.

[Report, 2012] Report, E. (2012). Air quality in Europe - 2012 report. *European Environment Agency*, 4.

[Roedel and Wagner, 2011] Roedel, W. and Wagner, T. (2011). *Physik unserer Umwelt: Die Atmosphäre - Aerosole*.

[RUC - NOAA, 2020] RUC - NOAA (2020). Aerosol module (MADE-SORGAM). `https://ruc.noaa.gov/wrf/wrf-chem/made_sorgam.htm`.

[Schell, 2000] Schell, B. (2000). Die Behandlung sekundärer organischer Aerosole in einem komplexen Chemie-Transport-Modell. *Mitteilungen aus dem Institut für Geophysik und Meteorologie der Universität zu Köln*, no. 135.

[Schell et al., 2001] Schell, B., Ackermann, I. J., Hass, H., Binkowski, F. S., and Ebel, A. (2001). Modeling the formation of secondary organic aerosol within a comprehensive air quality model system. *Journal of Geophysical Research: Atmospheres*, 106.

[Skamarock et al., 2008] Skamarock, W. C., Klemp, J. B., Dudhia, J., Gill, D. O., Barker, D. M., Duda, M. G., Huang, X., Wang, W., and Powers, J. G. (2008). A description of the advanced research WRF version 3. *NCAR, Tech. Note*.

[Umweltbundesamt, 2020] Umweltbundesamt (06.04.2020). Staub - allgmein). `https://www.umweltbundesamt.at/umweltsituation/luft/luftschadstoffe/staub/`.

[Whitby, 1978] Whitby, K. T. (1978). The physical characteristics of sulfur aerosols. *Atmospheric Environment*, 12.

[Wild et al., 2000] Wild, O., Zhu, X., and Prather, M. (2000). Fast-J: Accurate Simulation of In- and Below-Cloud Photolysis in Tropospheric Chemical Models. *Journal of Atmospheric Chemistry*, 37:245–282.

[Wilks, 2011] Wilks, D. S. (2011). *Statistical methods in the atmospheric sciences - Third edition*. Elsevier Academic Press.